Neutron Dosimetry of Mice Using Monoenergetic Neutron Beams

by

Brent Alan Fallin

Medical Physics Program
Duke University

Date:_____
Approved:

_____
Calvin Howell, Supervisor

_____
Timothy Turkington

_____
Robert Reiman

Thesis submitted in partial fulfillment of
the requirements for the degree of Master of Science in the
Medical Physics Program in the Graduate School
of Duke University

2011

ABSTRACT

Neutron Dosimetry of Mice Using Monoenergetic Neutron Beams

by

Brent Alan Fallin

Medical Physics Program
Duke University

Date:_____
Approved:

_____
Calvin Howell, Supervisor

_____
Timothy Turkington

_____
Robert Reiman

An abstract of a thesis submitted in partial
fulfillment of the requirements for the degree
of Master of Science in the
Medical Physics Program in the Graduate School
of Duke University

2011

Copyright by
Brent Alan Fallin
2011

Abstract

In 2009 the researchers at Triangle Universities Nuclear Laboratory (TUNL) participated in a series of experiments with the Radiation Countermeasures Center of Research Excellence (RadCCORE). This thesis project is a component of the research done at TUNL that was partially supported by the RadCCORE collaboration. The primary goals of this work are: (1) to measure the neutron fluence (and hence the dose) from the standard neutron beam source at TUNL delivered to a small animal target to an accuracy of better than ± 10% and (2) to develop techniques for real time monitoring of the absolute dose delivered to small animal targets from neutron beam irradiation. These two projects are interconnected as the development of the real-time monitoring techniques depends on the results of the absolute fluence measurements.

Measuring the absolute neutron beam fluence necessitates the use of a reaction in which the neutron cross section is accurately known over the relevant energy range and a detection technique which is insensitive to gamma-rays or is capable of distinguishing gamma-rays from neutrons. In this work, neutron activation of aluminum and gold foils was used to make absolute measurements of the fast neutron (E_n ~ 10 MeV) fluence. Neutron activation of gold foils was also used to make a relative measurement of the thermal neutron fluence. The neutrons produced nuclear reactions in the foils, converting a small quantity of the stable atoms in the foils into radioactive ones which subsequently generate gamma-rays in their decay process. The activated foils are then removed from the beam and placed in front of a high-purity germanium (HPGe) detector that measures the energy spectrum of the gamma-rays emitted by the foil. By counting the number of gamma-rays detected over a set time, the incident neutron fluence at the foil location was

determined using the known reaction cross sections. The measured neutron fluence was used to calculate the imparted dose to live mouse targets via the muscle tissue neutron kerma factors. Liquid and plastic scintillation detectors were also used to monitor the relative neutron flux in real time during the experiments. These relative detectors were subsequently calibrated using flux results obtained from the foil activation measurements and were used for real time dose monitoring.

The neutron beam produced at TUNL also has an intrinsic gamma component that adds to the dose received by a small animal target. The gamma contribution to imparted dose is generally taken to be around 10% or less for neutron beams created by linear accelerators utilizing the $^{2}H(d,n)^{3}He$ reaction[1], but no confirming measurements of this type have been performed at TUNL prior to this work. To verify this claim, an experiment was conducted to quantify the gamma-ray contribution to the target dose at several incident neutron energies and gas cell pressures.

The dosage from the mixed beam was measured using two ionization chambers that have different sensitivities to neutron and gamma radiation. The chambers were placed in the neutron beam, and the total charge induced in the ionization chamber by the mixed radiation field was monitored. The percent gamma-ray contribution to total target dose was calculated utilizing the procedures outlined in AAPM Report No. 7[2] and Attix[3].

Using the foil activation technique, the neutron fluence incident on target and dose delivered were measured to within ± 10%. The target dose estimated using the scintillation detectors was found to be accurate to within ± 20%. The results of the ion

[1] ICRU Report 26 (pg. 25,48)
[2] AAPM Report No. 7
[3] Attix (Chapter 16)

chamber measurements imply the gamma-ray component of the neutron beam at TUNL contributes less than 5% to the total target dose. Given the large difference in quality factors between gamma-rays (=1) and fast neutrons (~10), the contribution by gamma radiation to the total equivalent dose was determined to be negligible.

Dedication

I would not have had the opportunity to complete my graduate studies here at Duke without the generosity of many individuals at Triangle Universities Nuclear Laboratory (TUNL) over the years. I would first like to thank Dr. John Kelley and Dr. Henry Weller for giving me the opportunity to gain my first research experience at Duke as part of TUNL's Research Experience for Undergraduates (REU) program in the summer of 2003. It was through this program that I gained a love of nuclear physics and the encouragement to continue my studies at Duke subsequent to my graduation. I am also eternally grateful and indebted to Dr. Werner Tornow for seeing my potential as a researcher, always believing in me, and being adamant that I not leave TUNL without a degree in hand. I gained invaluable experience in nuclear physics research from him and Dr. Anton Tonchev during my employment as a Research Associate at TUNL for the 5 years before I began my current program of study. I would like to thank the current Director of TUNL, Dr. Calvin Howell, for first encouraging me to enter into Duke's Medical Physics Graduate Program and for all of his generous support while I have pursued my graduate studies these last several years. I would also like to thank the Radiation Safety Officer, Chris Westerfeldt, and all the technical staff at TUNL: Paul Carter, Richard O'Quinn, John Dunham, and Jeff Addison. Without all your hard work, research at this laboratory would not be possible. Your encouragement and friendship have been invaluable to me and is something I will always treasure. Thank you. Last, but certainly not least, I would like to thank my Lord and Savior, Jesus Christ, without whom this work could not have been accomplished. "I can do all things through Christ who strengthens me." Philippians 4:13 NKJV

Contents

Abstract iv

List of Tables xi

List of Figures xiii

1. Introduction 1

    1.1 Motivation 1

    1.2 Triangle Universities Nuclear Laboratory 1

    1.3 RadCCORE Project 6

2. Foil Activation Technique 8

3. Low Background Gamma-Ray Counting Area 15

4. Neutron Fluence Determination 19

5. Detector Efficiency Measurement 23

6. January 2009 RadCCORE Experiment 25

    6.1 Experiment Setup and Description 25

    6.2 Results 29

    6.3 Discussion and Summary 32

7. April 2009 RadCCORE Experiment 34

    7.1 Experiment Setup and Description 34

    7.2 Results 37

    7.3 Discussion and Summary 38

8. May 2009 RadCCORE Experiment 40

    8.1 Experiment Setup and Description 40

    8.2 Results 44

8.3 Discussion and Summary 45

9. July 2009 RadCCORE Experiment 47

9.1 Experiment Setup and Description 47

9.2 Results 52

9.3 Discussion and Summary 54

10. RadCCORE Summary 56

10.1 Final Observations 56

10.2 Possibilities for the Future 58

11. Ionization Chamber Measurement 60

11.1 Introduction 60

11.2 Ionization Chamber Descriptions and Theory 60

11.3 Experiment Setup and Description 63

11.4 Analysis 66

11.5 Results 75

11.6 Discussion and Summary 77

11.7 Future Improvements for Ionization Chamber Measurements at TUNL 80

12. Concluding Remarks 81

Appendix A - Foil Measurement Sources of Error 82

Appendix B – Detector Efficiency Curves 83

Appendix C - Dose Estimation Using an Off-Axis Liquid Scintillation Detector 87

Appendix D - Dose Estimation Using a Plastic Scintillator Paddle at 0° 89

Appendix E – Principal Kerma Producing Reactions in Tissue 91

Appendix F - Gamma Dose Fraction Measurement Sources of Error 94

References 95

List of Tables

Table 6.2.1. January 2009 Run – Results of the $^{27}Al(n,\alpha)^{24}Na$ Activation Foil Measurement. 30

Table 6.2.2. January 2009 Run – Results of the $^{197}Au(n,2n)^{196}Au$ Activation Foil Measurement. 30

Table 6.2.3. January 2009 Run – Reduction in Fast Neutron Flux Across the Water Target Determined Using Al Activation Foils. 31

Table 6.2.4. January 2009 Run – Reduction in Fast Neutron Flux Across the Water Target Determined Using Gold Activation Foils. 31

Table 6.2.5. January 2009 Run – Results of the $^{197}Au(n,\gamma)^{198}Au$ Activation Foil Measurement. 31

Table 6.2.6. Slow Neutron Flux Reduction by the Cd Shell Based on Al Activation Foil Normalization. 31

Table 6.2.7. Slow Neutron Flux Reduction by the Cd Shell Based on Au Activation Foil Normalization. 31

Table 6.2.8. Average (Al and Au foils) of Slow Neutron Flux Reduction by the Cd Shell. 32

Table 7.1.1. April 2009 Run – Setup Data. 37

Table 7.2.1. April 2009 Run – Results of the $^{27}Al(n,\alpha)^{24}Na$ Activation Foil Measurement. 38

Table 7.2.2. April 2009 – Reduction in Fast Neutron Flux Across the Water Target Determined Using Al Activation Foils. 38

Table 7.2.3. Reduction in Fast Neutron Flux at Off-Axis Position Compared to 0º. 38

Table 8.1.1. May 2009 Run – Setup Data. 43

Table 8.2.1. May 2009 Run – 200 cGy Irradiation Data. 45

Table 8.2.2. May 2009 Run – 50 cGy Irradiation Data. 45

Table 9.1.1. July 2009 Run – Setup Data. 48

Table 9.2.1. July 2009 Run – Results of the $^{27}Al(n,\alpha)^{24}Na$ Activation Measurement. 53

Table 9.2.2. July 2009 Run – Calculated Dose to Target 53

Table 11.2.1. Percent By Mass Elemental Composition of TE Plastic, TE Gas, and ICRU 46 Muscle. 61

Table 11.3.1. Ionization Chamber 8 MeV Irradiation Run Data. 65

Table 11.3.2. Ionization Chamber 10 MeV Irradiation Run Data. 65

Table 11.4.1. TE-TE and C-CO_2 Relative Sensitivities by Neutron Energy. 70

Table 11.4.2. ^{12}C(n,total) Cross Sections and Attenuation Corrections by Neutron Energy. 73

Table 11.5.1. Collected charge, R', and R' w/ neutron attenuation correction for the TE-TE chamber as a function of neutron energy and gas cell pressure. 76

Table 11.5.2. Collected charge, R', and R' w/ distance correction for the C-CO_2 Chamber as a function of neutron energy and gas cell pressure. 76

Table 11.5.3. Gamma dose fraction as a function of neutron energy and gas cell pressure for experimentally determined values of k_T and k_u and for $k_T = 1$. 77

Table 11.5.4. Neutron fluences and corresponding derived doses (using neutron kerma factors for muscle tissue) at Foil 1 (in front of C-CO_2) and Foil 2 (in front of TE-TE) positions. 77

Table 11.5.5. Foil 2 (in front of TE-TE) neutron dose corrected for distance and surface area vs. dose determined from the TE-TE Chamber. 77

Table A.1. Foil Measurement Sources of Error. 82

Table F.1. Gamma Dose Fraction Measurement Sources of Error. 94

List of Figures

Figure 1.2.1: Floor layout of the tandem laboratory at TUNL. 4

Figure 1.2.2: Neutron energy vs. laboratory angle for the $^{2}H(d,n)^{3}He$ reaction for 6.823 MeV deuterons. 5

Figure 1.2.3: $^{2}H(d,n)^{3}He$ differential cross section vs. laboratory angle for 6.823 MeV deuterons. 5

Figure 2.1. Nuclear decay scheme for ^{24}Na. 10

Figure 2.2. Cross section vs. neutron energy for the $^{27}Al(n,\alpha)^{24}Na$ reaction. 10

Figure 2.3. Cross section vs. neutron energy for the $^{197}Au(n,2n)^{196}Au$ reaction. 13

Figure 2.4. Nuclear decay scheme for ^{196}Au. 13

Figure 2.5. Cross section vs. neutron energy for the $^{197}Au(n,\gamma)^{198}Au$ reaction. 14

Figure 2.6. Nuclear decay scheme for ^{198}Au. 14

Figure 3.1. Schematic diagram of the foil counting holder. 17

Figure 3.2. Canberra 60% efficiency HPGe detector with lead brick shielding. 18

Figure 3.3. Canberra extended range 20% HPGe detector with shield. 18

Figure 6.1.1. Schematic diagram (side view) of the January 2009 RadCCORE setup..... 25

Figure 6.1.2. Target assembly used in the January 2009 RadCCORE experiment. 26

Figure 6.1.3. Cross section vs. neutron energy for the $^{113}Cd(n,\gamma)^{114}Cd$ reaction. 28

Figure 7.1.1. Test tube and water bottle target. 34

Figure 7.1.2. Mouse target holder diagram. 35

Figure 8.1.1. May 2009 activation foil starting and stopping positions. 42

Figure 9.1.1. Schematic diagram of the LN_2 gas cell designed for the fourth RadCCORE experiment. 50

Figure 9.1.2. July 2009 activation foil starting and stopping positions. 51

Figure 11.3.1. Ionization chamber setup. 63

Figure B.1. Detector 1 Efficiency Curve – January 2009. 83

Figure B.2. Detector 3 Efficiency Curve – January / May 2009. 83

Figure B.3. Detector 1 Efficiency Curve – April 2009. 84

Figure B.4. Detector 2 Efficiency Curve – April 2009. 84

Figure B.5. Detector 1 Efficiency Curve – July 2009. 85

Figure B.6. Detector 2 Efficiency Curve – July 2009. 85

Figure B.7. Detector 3 Efficiency Curve – July 2009. 86

Figure B.8. Detector 1 Efficiency Curve – January 2010. 86

Figure E.1. Cross section vs. neutron energy for the ^{1}H(n,elastic) reaction. 91

Figure E.2. Cross section vs. neutron energy for the ^{12}C(n,elastic) reaction. 92

Figure E.3. Cross section vs. neutron energy for the ^{12}C(n,inelastic) reaction. 92

Figure E.4. Cross section vs. neutron energy for the ^{16}O(n,elastic) reaction. 93

Figure E.5. Cross section vs. neutron energy for the ^{16}O(n,inelastic) reaction. 93

1. Introduction

1.1 Motivation

Mixed field dosimetry involving fast-neutron and gamma-ray components is an area of growing interest within the scientific community. Individuals in the general population could potentially be exposed to a significant radiation dose from a mixed field source as a result of a nuclear reactor accident or from detonation of a nuclear device. Rapid assessment and screening of large numbers of individuals seeking treatment at local and regional medical centers will be necessary to sort out those exposed to high levels of radiation from those with little or no exposure. In order to make such determinations possible, the biological and hematological effects resulting from exposure to mixed neutron / gamma-ray radiation fields have been studied in small animals such as mice. Such experiments require the imparted dose to be known to a high degree of accuracy (± 10%). Since the dose imparted to soft tissues by neutron radiation is a function of the neutron energy, high precision dose measurements require the energy distribution of the neutron field to be well known. A quasi-monoenergetic neutron source such as is available at the Triangle Universities Nuclear Laboratory (TUNL) is well-suited for conducting neutron dosimetry research.

1.2 Triangle Universities Nuclear Laboratory

Triangle Universities Nuclear Laboratory is an inter-institutional research consortium between Duke University, North Carolina State University, and the University of North Carolina at Chapel Hill. The laboratory has historically engaged in basic science research, but has moved in recent years toward increasing the amount of applied research conducted by the consortium. The 10 MV tandem van de Graaff

accelerator combined with the Direct Extraction Negative Ion Source (DENIS) provides the capability of delivering beams of unpolarized protons and deuterons on targets at energies up to approximately 20 MeV.

To produce a proton or deuteron beam, a combination of hydrogen and deuterium gas is injected into the ion source, and negatively charged ions are then accelerated over a 50 kV potential difference. Protons or deuterons are preferentially selected for injection into the tandem using a dipole magnet located between DENIS and the tandem. Once the ions enter the tandem, they are accelerated toward the central positively charged terminal. A thin carbon foil located in the terminal strips away the electrons causing the now positively charged ions to be accelerated away from the terminal. This dual acceleration causes the ions to receive a total kinetic energy of twice the terminal voltage multiplied by the electric charge. Once exiting the tandem, the beam is momentum analyzed and bent into a particular beam line using a dipole magnet. A diagram of the TUNL facility can be seen in **Figure 1.2.1**.

For this work, a deuteron beam produced using the DENIS (labeled as "DENIS II" in the figure) was tuned down the 38° beam line into the Neutron Time-of-Flight (NTOF) target room where neutrons were produced via the $^{2}H(d,n)^{3}He$ reaction, in which accelerated deuterium ions are impinged on a gas cell pressurized with deuterium gas. Each reaction produces one atom of ^{3}He and a free neutron. The monoenergetic incident deuterons lose energy as they pass through the gas cell containment foil and a varying amount of deuterium gas before interacting, resulting in a range of neutron energies being produced. The amount of energy lost per unit length depends on the gas mass thickness, which is a function of the gas temperature and pressure (i.e. PV = nRT). The energy

spread resulting from the gas thickness is typically 300-500 keV for the deuterium pressures used in this work. The neutron energy at the center of the gas cell and the energy spread were calculated for each experiment using the TUNL computer code MAGNET[1]. The energy of the neutrons produced also depend on the angle at which they are ejected. The neutron energy as a function of lab angle was computed using the nuclear reaction kinematics code RKIN[2]. The neutron flux also varies with angle due to the angular dependence of the $^{2}H(d,n)^{3}He$ differential cross section. The differential cross section as a function of lab angle was calculated using the code DROSG-2000[3]. Plots of the neutron energy and differential cross section as a function of the lab angle for 6.823 MeV incident deuterons are shown in **Figures 1.2.2 and 1.2.3**.

[1] Roberts
[2] Manglos
[3] Drosg

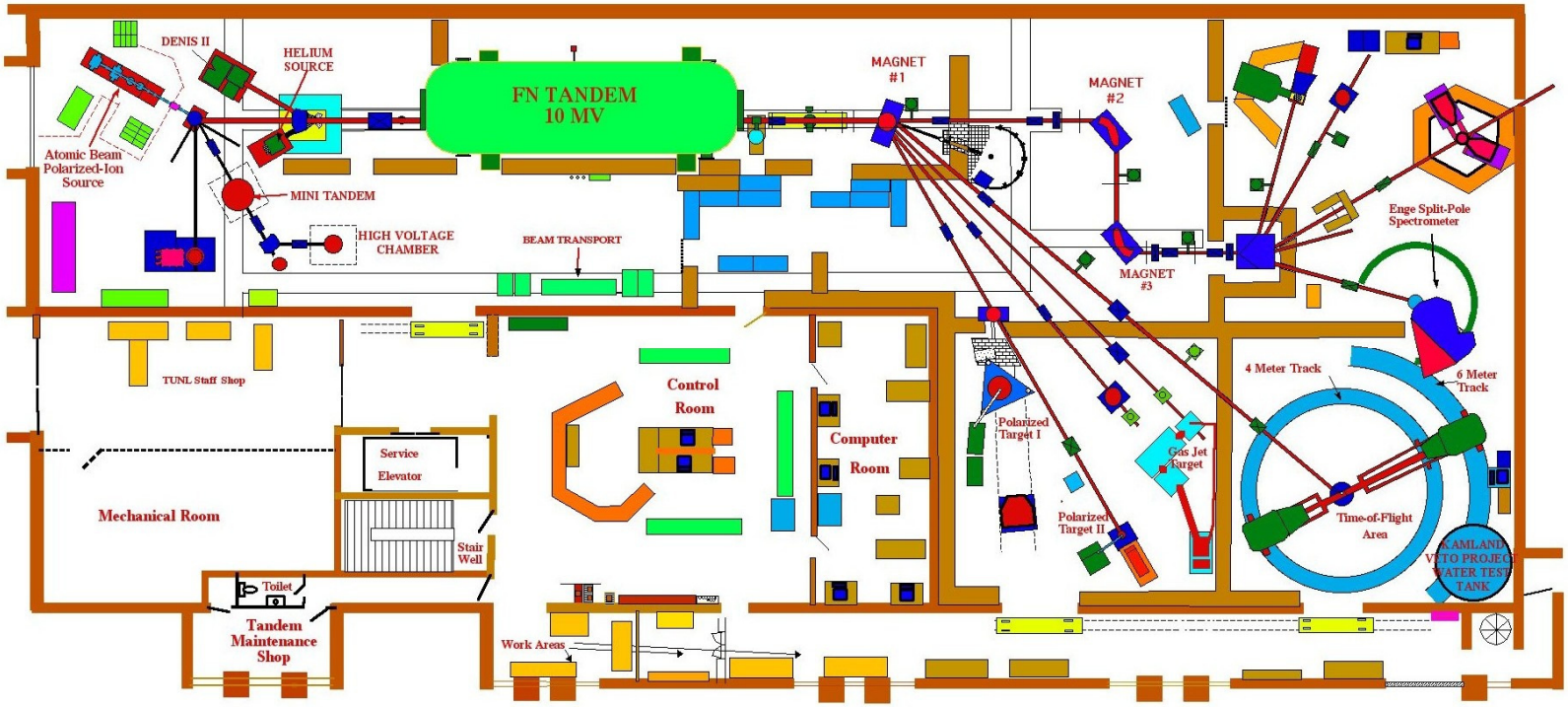

Figure 1.2.1: Floor layout of the tandem laboratory at TUNL.

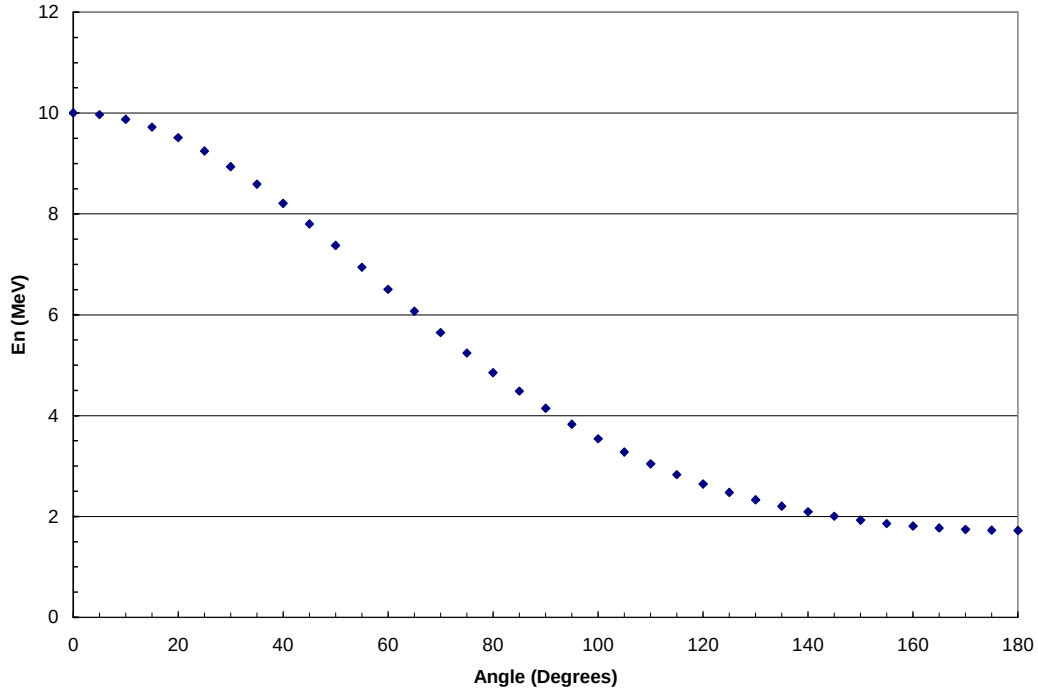

Figure 1.2.2: Neutron energy vs. laboratory angle for the $^{2}H(d,n)^{3}He$ reaction for 6.823 MeV deuterons.

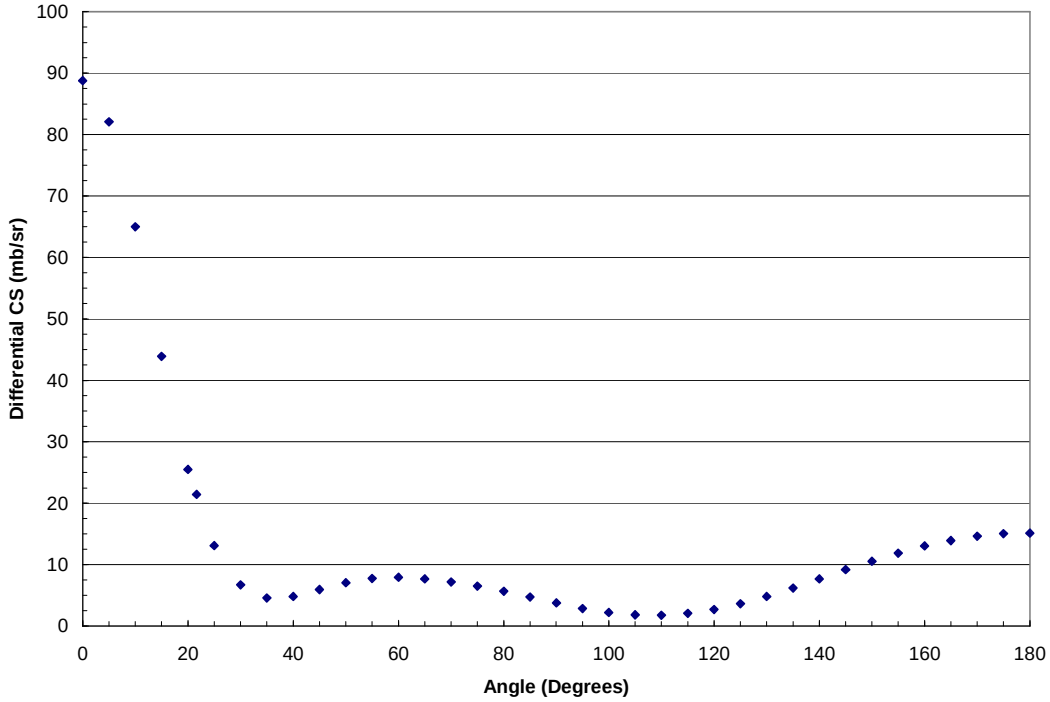

Figure 1.2.3: $^{2}H(d,n)^{3}He$ differential cross section vs. laboratory angle for 6.823 MeV deuterons.

1.3 RadCCORE Project

The first RadCCORE experiment was conducted in January 2009. The goals of the experiment were: (1) to use two different activation foils (aluminum and gold) to measure the fast and thermal neutron fluence incident upon a water bottle target (i.e. a mouse phantom), (2) to measure the attenuation of fast neutrons through the phantom, (3) to use cadmium plating to determine the relative contribution of thermal neutrons to the slow neutron fluence, and (4) to cross calibrate the foil activation results with the optical density change in Gafchromic® (Ashland Specialty Ingredients, Wayne, NJ) dosimetry film. The calibration and analysis of Gafchromic® film for use in neutron dosimetry is not part of the present work. The reader is directed to the doctoral thesis of Samuel Brady for a thorough description of this topic[4]. The goals of the second RadCCORE experiment performed in April 2009 were: (1) to measure the attenuation of the neutron beam through the mouse phantom on the central beam axis using a new target holder assembly and (2) to compare the neutron fluence incident upon a target placed on the central axis (i.e. 0º) to that incident upon an identical target placed in an off-axis position. For the third RadCCORE experiment, conducted in May 2009, live mouse targets were irradiated in the neutron beam in six symmetric off-axis positions using the new target holder. Two separate sets of mice were irradiated with goal neutron doses of 200 cGy and 50 cGy, respectively. For the fourth RadCCORE experiment, performed in July 2009, a newly constructed liquid nitrogen cooled gas cell was used to produce the neutron beam. This target increased the effective thickness of the deuterium gas target by about a factor of four, thus producing a significantly higher neutron flux for faster dose delivery. Nine sets

[4] Brady

of mice were irradiated in this experiment, three sets each at goal doses of 50 cGy, 200 cGy, and 500 cGy, respectively. The average 0° neutron energies were 10.16 MeV for the first RadCCORE experiment, 10.00 MeV for the second and third experiments, and 10.21 MeV for the fourth experiment.

2. Foil Activation Technique

A foil activation technique was used to passively monitor the neutron fluence incident on the water bottle and mouse targets. Aluminum and gold foils (2.5 cm diameter and 100 μm thick) were used in the experiments detailed in this work. When aluminum is struck by neutrons with an energy higher than 3.249 MeV, the $^{27}Al(n,\alpha)^{24}Na$ reaction can occur. In this reaction an aluminum nucleus absorbs a neutron and emits an α particle, thereby converting the aluminum (which is naturally 100% ^{27}Al) into ^{24}Na. The probability for this reaction occurring is a function of the reaction cross section which depends on the energy of the incident neutron. The cross section is usually measured in units of barns (b), where one barn is equal to $1x10^{-24}$ cm^2. Since the $^{27}Al(n,\alpha)^{24}Na$ cross section drops off rapidly with decreasing neutron energy and is zero below 3.249 MeV (the reaction threshold), thermal neutrons do not contribute to the production of ^{24}Na, making it an ideal reaction for monitoring for the flux of the fast-neutron component in the beam.

The ^{24}Na nuclei which are produced by the $^{27}Al(n,\alpha)^{24}Na$ reaction are radioactive and decay by β^- emission to ^{24}Mg (which is stable). The half-life of ^{24}Na is 14.997 ± 0.012 hours. After undergoing β^- decay, the residual ^{24}Mg nucleus emits gamma-rays at several distinct energies, depending on the spin of the excited state of ^{24}Mg produced, in order to return to its ground state energy level. The highest intensity β^- decay (99.855%) path is to the 4^+ excited state of ^{24}Mg, which subsequently decays to the ground state by sequential emission of 2754 keV and 1369 keV gamma-rays. The decay scheme for ^{24}Na

and the cross section for the $^{27}Al(n,\alpha)^{24}Na$ reaction from threshold up to 20 MeV are shown in **Figures 2.1 and 2.2**, respectively.[1]

[1] National Nuclear Data Center (NNDC). All cross section plots in this work are taken from "σigma." Cross section values were taken from "ENDF." All decay scheme plots and corresponding gamma energies were taken from "NuDat 2.5."

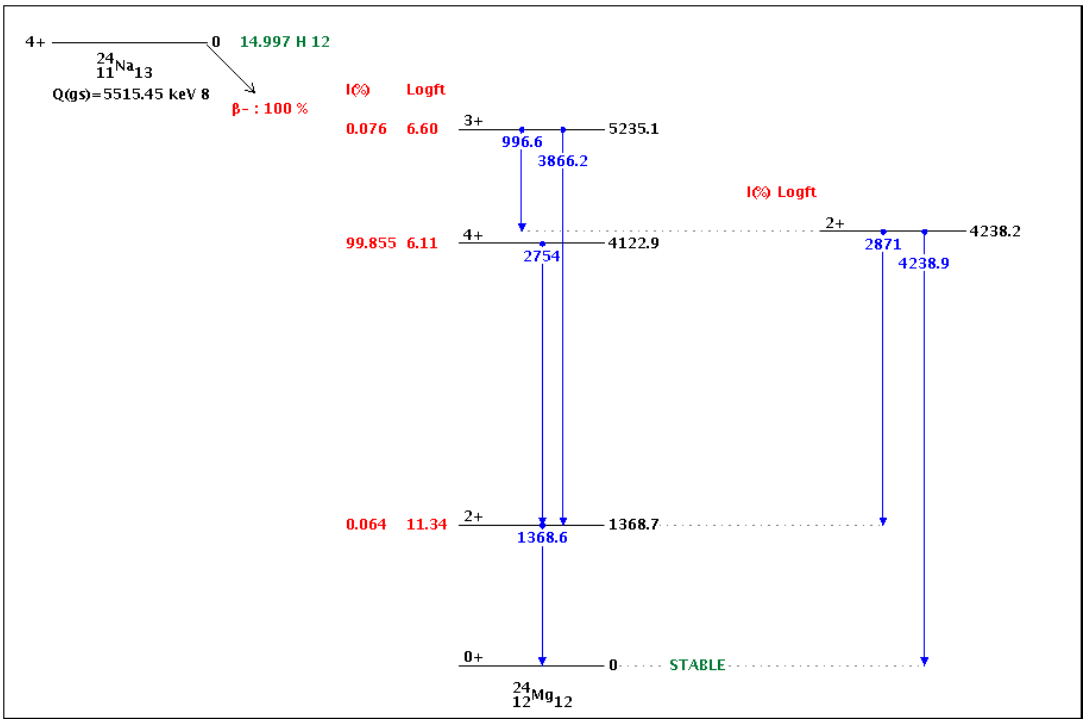

Figure 2.1. Nuclear decay scheme for ^{24}Na.

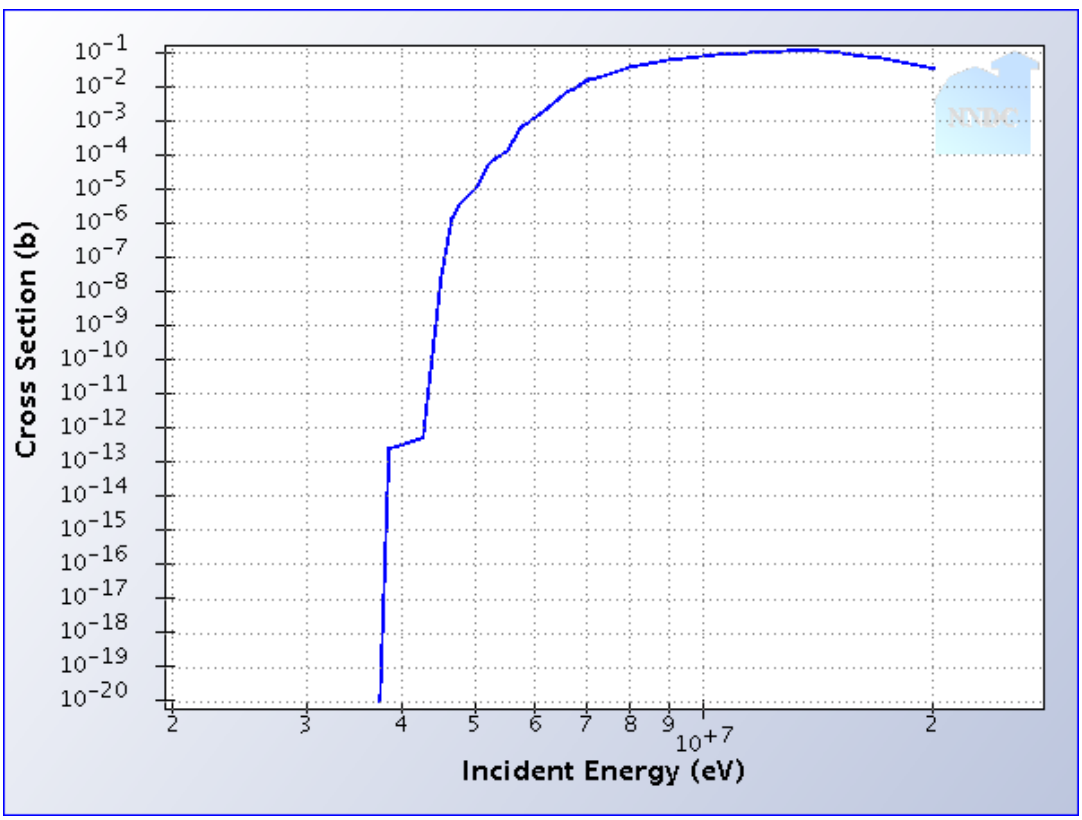

Figure 2.2. Cross section vs. neutron energy for the ^{27}Al(n,α)^{24}Na reaction.

For the first RadCCORE experiment in January 2009, gold foils were also used to monitor both the fast and slow (E_n < 0.4 eV) neutron components of the beam. Gold, like aluminum, is naturally monoisotopic (100% ^{197}Au). The ^{197}Au(n,2n)^{196}Au reaction, which has a threshold of 8.114 MeV, converts ^{197}Au into ^{196}Au, which subsequently decays by electron capture into ^{196}Pt with a half-life of 6.1669 ± 0.0006 days. Because the energy of the incident neutrons exceeded this threshold, this reaction was used to cross check the flux results obtained from the aluminum foil measurements. The most intense transition (87%) in the decay of ^{196}Au is to the 2^+ excited state of ^{196}Pt which subsequently decays to the ground state through emission of a 356 keV gamma-ray. At 10.16 MeV, the cross section for ^{197}Au(n,2n)^{196}Au is 1.036 b, more than an order of magnitude higher than the corresponding cross section for ^{27}Al(n,α)^{24}Na. The efficiency of the detectors used to count the monitor foils is also significantly higher at 356 keV than at 1369 keV. Given similar measurement times, the counting statistics for the gold 356 keV gamma-ray peak are much better than for the aluminum 1369 keV line. Regardless, the ^{27}Al(n,α)^{24}Na reaction is still the preferred standard for the present fast neutron measurements since its cross section varies much less over the energy range of neutrons produced by the gas cell than that of the ^{197}Au(n,2n)^{196}Au reaction.

Gold foils are most frequently used as a monitor for slow neutrons. The neutron capture reaction converts ^{197}Au into ^{198}Au, which subsequently decays by β^- emission into ^{198}Hg with a half-life of 2.6947 ± 0.0003 days. The highest intensity transition in that decay (98.990%) is to the 2^+ excited state of ^{198}Hg which subsequently decays to the ground state energy level by emission of a 412 keV gamma-ray. There is no threshold energy for this reaction to occur, and at thermal neutron energies (v_n ~ 2200 m/s → KE ~

0.0253 eV), the capture cross section is approximately 100 barns; above 10 keV, the capture cross section drops off rapidly. Thus, fast neutrons contribute negligibly to the overall reaction yield. An absolute measurement of the thermal neutron flux requires precise knowledge of the slow neutron energy distribution at the target position. As this information was not available, the slow neutron flux measured with the gold foils was intrinsically relative. Since only the ability to observe changes in the slow neutron flux in different conditions was desired, a relative measurement was sufficient for the purposes of this experiment. Cross section plots for production of ^{196}Au and ^{198}Au and their associated decay schemes are shown in **Figures 2.3, 2.4, 2.5, and 2.6**.

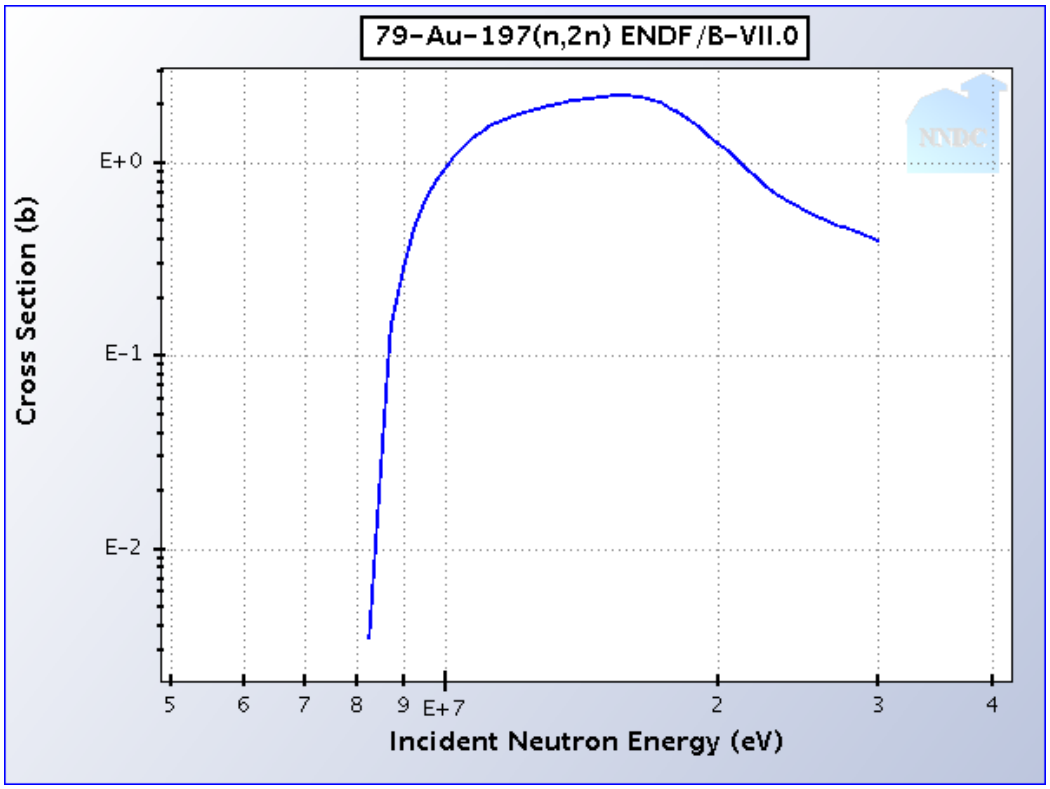

Figure 2.3. Cross section vs. neutron energy for the ^{197}Au(n,2n)^{196}Au reaction.

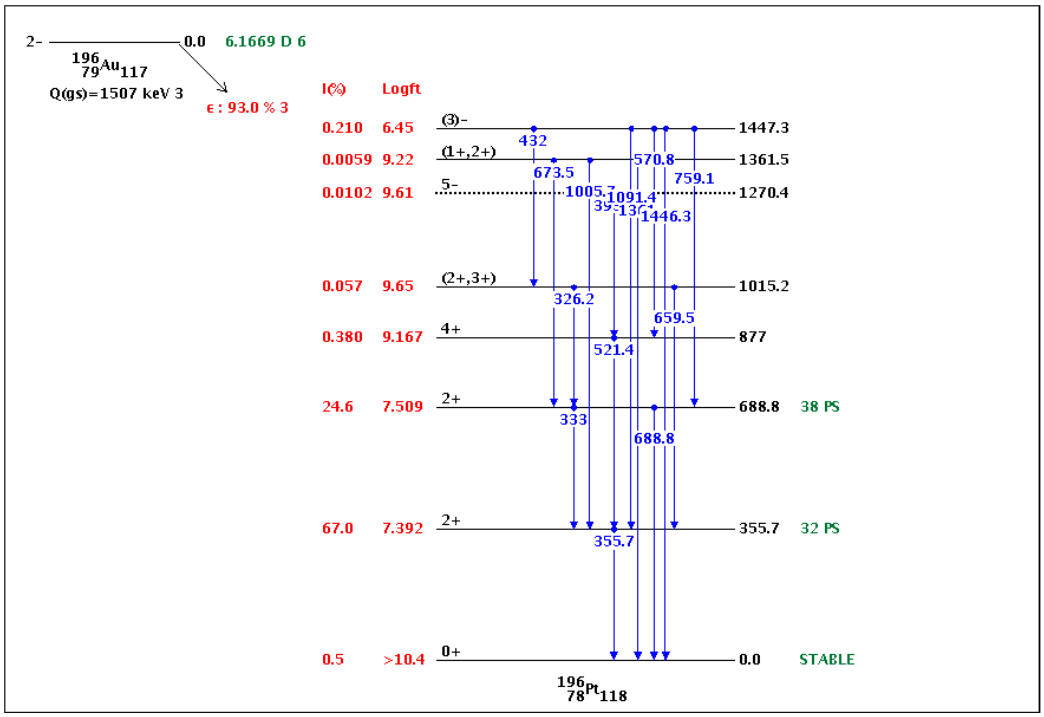

Figure 2.4. Nuclear decay scheme for ^{196}Au.

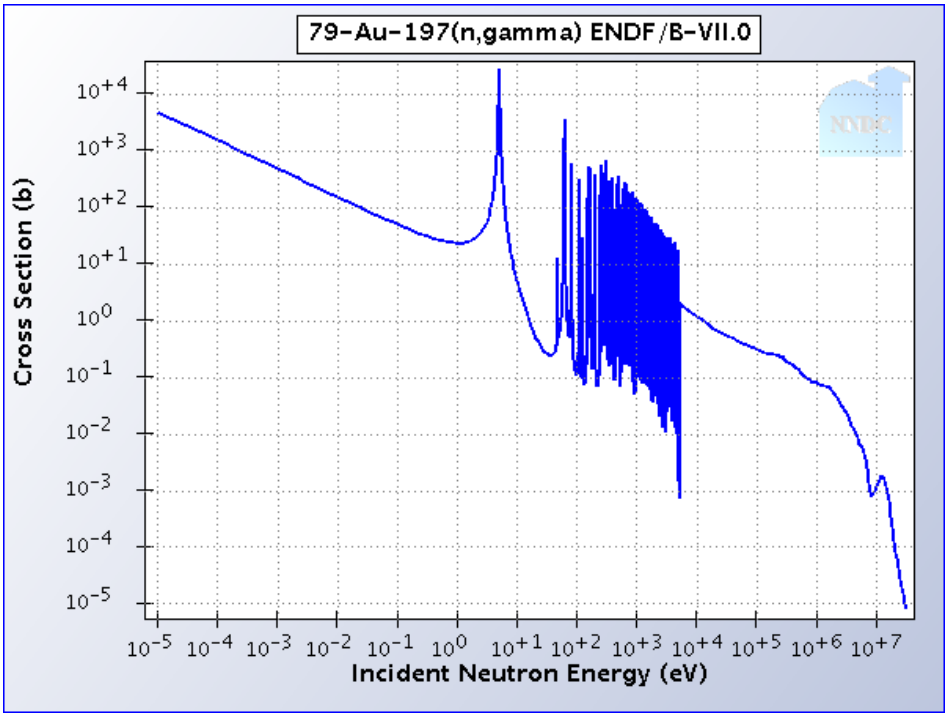

Figure 2.5. Cross section vs. neutron energy for the $^{197}Au(n,\gamma)^{198}Au$ reaction.

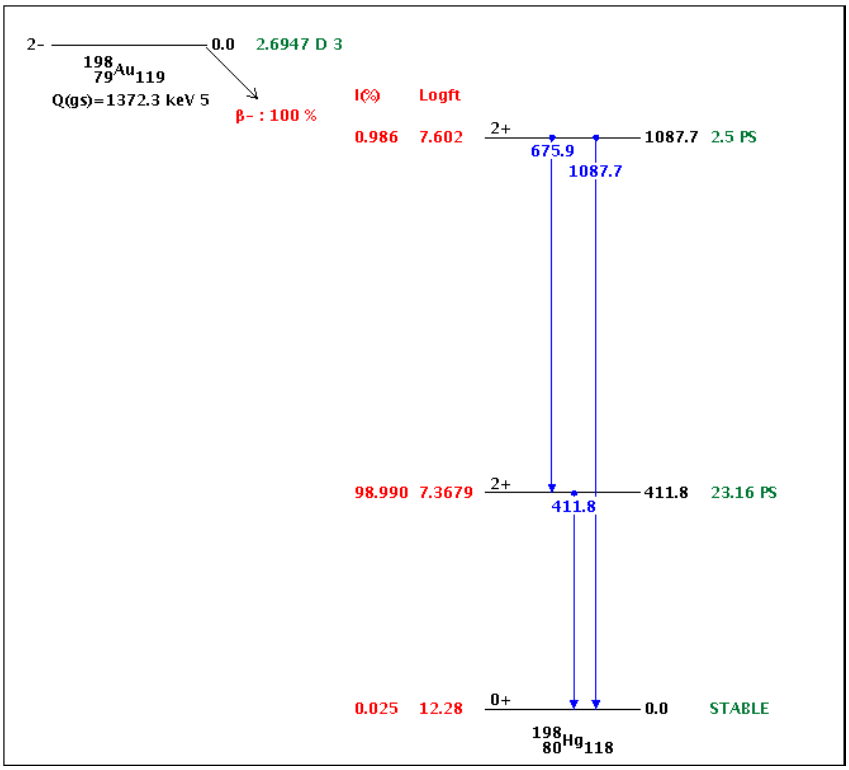

Figure 2.6. Nuclear decay scheme for ^{198}Au.

3. Low Background Gamma-Ray Counting Area

The counting portion of the foil activation measurements was carried out in the Low Background Counting Area, located in the basement of the Physics building adjacent to TUNL's Laboratory for Experimental Nuclear Astrophysics (LENA). Each foil to be counted was individually placed within a target holder (see **Figure 3.1**) and positioned in front of a background-shielded HPGe detector. Several different HPGe detectors were used in these measurements: two Canberra (Canberra Industries, Meridian, CT) 60% HPGe detectors (Model: GC6021) and one Canberra Extended Range 20% HPGe detector (Model: GX2020). The foil targets measured using the 60% detectors were placed 2 cm from the front face of the detector. The foils measured using the 20% detector were placed 3 cm from the detector face. The two 60% HPGe detectors were background shielded with custom made lead enclosures that surrounded the detector crystal, while the 20% HPGe detector was shielded with a cylindrical commercial shield made by Canberra. The two detectors and corresponding shields can be seen in **Figures 3.2 and 3.3**, respectively.

The detectors output signals were connected to Canberra 2026 Spectral Amplifiers which were gain adjusted to provide a full scale energy range of approximately 2 MeV. The amplifier output was then fed into a Canberra Multiport II Multi-channel Analyzer which was connected to a data acquisition machine utilizing Canberra's GENIE 2000 Gamma Acquisition and Analysis software. The foils were measured for sufficient time to obtain adequate counting statistics (~ 1% - i.e. >10000 counts) in the full energy photopeak of the gamma-ray of interest. The spectra were saved

as single column ASCII files (16384 channels) and analyzed in the spectroscopy program TV[1].

[1] Fitzler

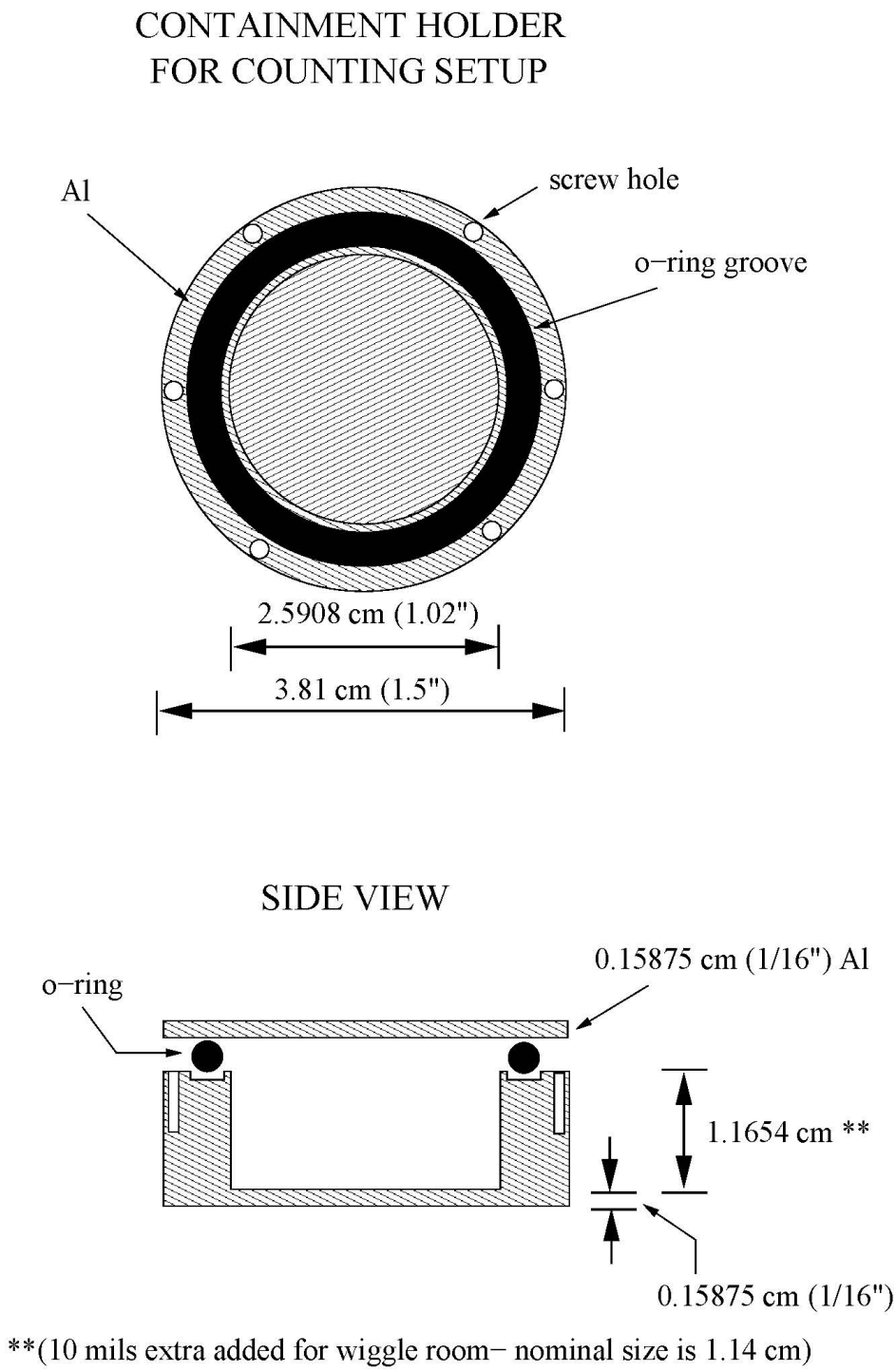

Figure 3.1. Schematic diagram of the foil counting holder.

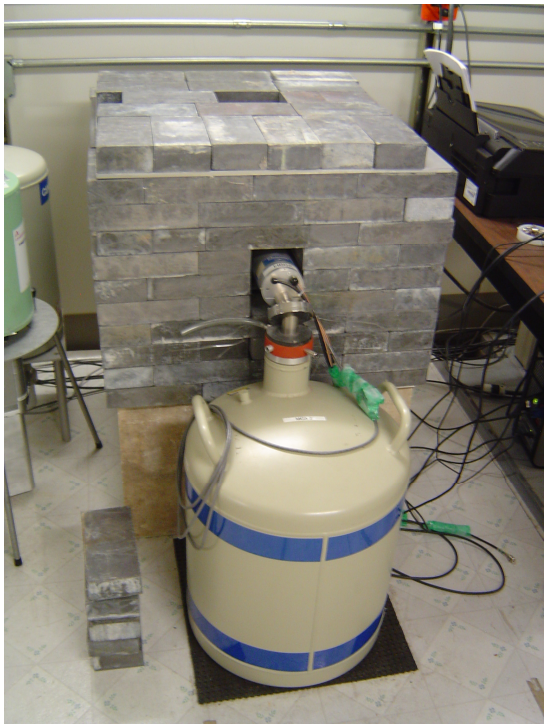

Figure 3.2. Canberra 60% efficiency HPGe detector with lead brick shielding.

Figure 3.3. Canberra extended range 20% HPGe detector with shield.

4. Neutron Fluence Determination

Determination of the neutron fluence by the foil activation technique required detailed measurements of several beam, foil, and detector parameters. Prior to activation, the aluminum and gold foils were carefully weighed on a digital scale (AT261 DeltaRange®, Mettler Toledo, Inc., Columbus, OH) capable of measuring object weights to an accuracy of ± 0.01 milligrams. Several conversion reactions on ^{27}Al are possible at 10 MeV incident neutron energy, including (n,γ), (n,p), (n,d), (n,np), and (n,α). These reactions lead to the production of ^{28}Al, ^{27}Mg, ^{26}Mg (stable), and ^{24}Na, respectively. In gold, all of the aforementioned reaction channels are open as well as (n,2n) and (n,t). These reactions result in the creation of ^{198}Au, ^{197}Pt, ^{196}Pt (stable), ^{194}Ir, ^{196}Au, and ^{195}Pt (stable), respectively. The gamma-rays produced by decay of the additional isotopes do not interfere with those produced through decay of ^{24}Na, ^{196}Au, and ^{198}Au.

In addition to the foil weight and dimensions, the following quantities necessary for the calculation of the neutron fluence were measured directly: (1) the foil irradiation time, (2) the decay time subsequent to irradiation but prior to measurement, (3) the detector measurement time (i.e. “real time”) and electronic live time, (4) the detector efficiency at the gamma energy of interest (1369 keV for the aluminum foils, and 356 keV (^{196}Au) and 412 keV (^{198}Au) for the gold foils), and (5) the net photopeak counts in the gamma-ray line of interest. All other parameters used in the fluence calculation were constants referenced from the relevant authoritative sources. The following equation was used to calculate the neutron fluence (n/cm^2) through the target:

$$\Psi = \frac{C_{photo} \times t_{irr} \times \frac{\ln(2)}{t_{1/2}}}{\varepsilon_{\det} \times \Omega_{corr} \times N_{nuclei} \times I_{\gamma} \times CS(b) \times \frac{10^{-24} cm^2}{b} \times f_{absorb} \times f_{irr} \times f_{decay} \times f_{meas}}$$

where

C_{photo} is the net number of counts measured in the gamma photopeak,

t_{irr} is the irradiation time (in seconds),

ε_{det} is the detector efficiency at the gamma-ray energy of interest,

Ω_{corr} is a solid angle correction factor to account for the difference in diameter between the calibration sources used to measure the detector efficiency and the aluminum and gold foil diameters,

N_{nuclei} is the number of nuclei in the target foil,

I_{γ} is the branching ratio of the relevant gamma-ray,

CS(b) is the cross section (in barns) for the appropriate reaction at the incident neutron energy,

f_{absorb} is a correction factor accounting for absorption within the target foil of the gamma-rays emitted by the activation products,

f_{irr} is a correction factor accounting for the percent of maximum activity (at a given beam energy and current) created during irradiation,

f_{decay} is a correction factor accounting for the decay of the activation products that occurred subsequent to irradiation but before measurement, and

f_{meas} is a correction factor accounting for the limited decay of the activation products during measurement.

The preceding fluence equation can also be written in a more intuitive form as:

$$\Psi = \frac{A_{\infty} \times t_{irr}}{N_{nuclei} \times CS(cm^2)} \ ,$$

where A_{∞} is the saturation activity of the activation foil. The actual activity created by activation, A_0, is given by: $A_0 = A_{\infty} \times f_{irr}$.

The solid angle correction, Ω_{corr}, is equal to $\frac{\Omega_f}{\Omega_s}$, where Ω_f is the effective solid angle subtended by the detector at the source position for the activation foil, and Ω_s is the equivalent solid angle for the calibration source at the same position.

The effective solid angle for a disk source aligned along the longitudinal axis of a cylindrical detector is given by:

$$\Omega = \frac{4\pi a}{s}\int_0^\infty \frac{e^{-dk} J_1(sk) J_1(ak)}{k}\, dk\,,$$

where a is the detector radius, s is the source radius, d is the distance between the source and detector crystal, and the $J_1(x)$ are the 1st order Bessel functions of x[1]. This integral must be solved using numerical techniques.

The number of nuclei in the target foil is given by:

$$N_{nuclei} = \frac{m \times N_A \times I_{abun} \times S_{purity}}{A}\,,$$

where m is the foil mass (in grams), N_A is Avogadro's number (# atoms per mole), I_{abun} is the isotopic abundance (1.00 for both ^{27}Al and ^{197}Au), S_{purity} is the sample purity (99.5% for aluminum, 99.95% for gold), and A is the isotopic mass (in grams per mole).

The correction factors were calculated as follows:

$$f_{absorb} = \frac{1-e^{-(m_t \times m_{absorb})}}{m_t \times m_{absorb}}, \quad f_{irr} = 1 - e^{-\frac{\ln(2) t_{irr}}{\tau_{1/2}}}, \quad f_{decay} = e^{-\frac{\ln(2) t_{decay}}{\tau_{1/2}}}, \text{ and } f_{meas} = 1 - e^{-\frac{\ln(2) t_{meas}}{\tau_{1/2}}},$$

where m_t is the foil mass thickness (in g/cm^2), m_{absorb} is the mass absorption coefficient (in cm^2/g) for the gamma-ray emitted by activation product of interest in the foil medium, t_{irr}, t_{decay}, and t_{meas} are the irradiation time, decay time before measurement, and

[1] Knoll (pg. 119)

measurement time, respectively, and $\tau_{1/2}$ is the half-life of the relevant activation product. A detailed list of the percent uncertainties in the various quantities contained in the fluence calculation is given in **Appendix A**. The primary sources of uncertainty in these measurements are the detector efficiency at the gamma-ray energies of interest, and the reaction cross sections.

As was previously discussed, the energy and flux of the neutrons created by the $^{2}H(d,n)^{3}He$ reaction vary due to the angular dependence of the differential cross section and neutron energy. Since the foils were placed perpendicular to the gas cell and have finite size, the neutron energy varies slightly across the foil surface. For foils positioned along the 0° beam axis, the variation in the neutron energy across the foil surface is generally less than 100 keV when 10 MeV neutrons are produced at 0°. This variation is much smaller than the typical energy spread in the neutron beam due to the gas thickness in the production cell. For off-axis foil positions, the energy variation across the foil can be up to 500 keV (i.e. on the order of the energy spread due to the gas thickness in the production cell when the pressure is ~ 7.8 atm). To simplify analysis of the foil activation results, the cross section used to calculate the flux incident on each foil was taken to be the value corresponding to the energy of the neutrons incident on the center of the foil and originating from the center of the gas cell.

5. Detector Efficiency Measurement

Accurate calculation of the fast neutron fluence incident on the target foils requires a precise measurement of the efficiency of the HPGe detectors at the gamma-ray energies of interest. By using a variety of gamma emitting sealed sources of known activity, a corresponding efficiency curve can be derived for each detector. This curve can then be fit to an empirical function to determine the detector efficiency at any energy within the range from which the individual data points were derived. Direct measurement of the absolute detector efficiency at a given energy is always more desirable, but usually not practically achievable. To make a direct measurement, one must first have access to a calibrated source of known activity that emits gamma-rays at exactly the desired energy or sufficiently close so that the difference in efficiency between the measured and desired energy is negligible. The situation is further complicated by the fact that only a small number of radioisotopes are suitable for use in detector efficiency measurements due to half-life, cost, and other practical considerations.

Detector efficiency curves for this project were constructed using ^{22}Na, ^{60}Co, ^{137}Cs, and ^{152}Eu sealed sources produced by Isotope Products Laboratories, Valencia, CA. The uncertainty in the activity of the ^{22}Na and ^{137}Cs sources was ± 3.0% (3σ), while the uncertainty in the activity of the ^{60}Co source was ± 3.1% (3σ). The ^{152}Eu source was used to make relative efficiency measurements. The detector efficiency at each respective gamma-ray energy was calculated according to the following equation:

$$\varepsilon_{\det} = \frac{C_{photo} \times (\frac{RT}{LT}) \times \frac{\ln(2)}{\tau_{1/2}}}{I_{\gamma} \times A \times f_{meas}},$$

where

C_{photo} is the net number of counts measured in the gamma photopeak,

RT is the detector real time,

LT is the detector live time,

$\tau_{1/2}$ is the half-life of the relevant calibration source,

I_{γ} is the branching ratio of the relevant gamma-ray,

A is the activity of the relevant calibration source at the time of measurement, and

$$f_{meas} = 1 - e^{-\frac{\ln(2)t_{meas}}{\tau_{1/2}}},$$

where $\tau_{1/2}$ is the half-life of the relevant calibration source as before and t_{meas} is the source measurement time.

As the shape of the efficiency curve derived from a given source is generally independent of the source strength and distance from the detector, the ^{152}Eu measurements were thus able to be scaled to the absolute measurements from the ^{22}Na, ^{60}Co, and ^{137}Cs sources in order to obtain efficiency curves for each of the detectors used in the experiment in the energy range from 244-1408 keV. These efficiency curves are included in **Appendix B**.

6. January 2009 RadCCORE Experiment

The main goals of the RadCCORE series of experiments (conducted in January, April, May, and July 2009) were to measure the fast neutron fluence and dose from the neutron beam source at TUNL to an accuracy of better than ± 10% and to develop neutron beam diagnostic capabilities that enable real-time dose monitoring. These aims necessitate development of the capability to determine the dose delivered from the various beam components (fast neutron, slow neutrons, and gamma rays) individually.

The first RadCCORE experiment, conducted in January 2009, had the following objectives: (1) use a foil activation technique to measure the fast and thermal neutron fluence incident upon a mouse phantom, (2) measure the attenuation of the fast neutrons through the phantom, and (3) use cadmium plating to determine the relative contribution of thermal neutrons to the slow neutron fluence incident upon the phantom. A description of the experiment, techniques, and results for the January 2009 experiment are presented in this chapter.

6.1 Experiment Setup and Description

Schematic diagrams of the target box and target assembly for the first RadCCORE experiment are shown in **Figures 6.1.1** and **6.1.2**, respectively.

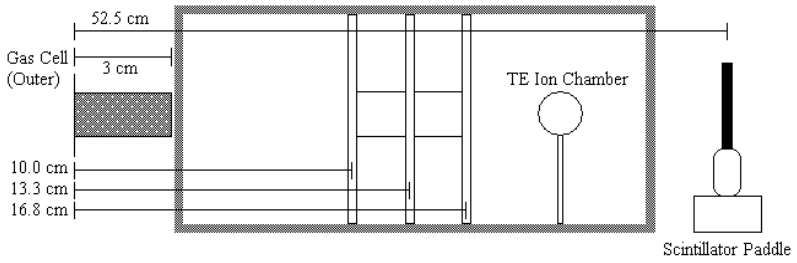

Figure 6.1.1. Schematic diagram (side view) of the January 2009 RadCCORE setup.

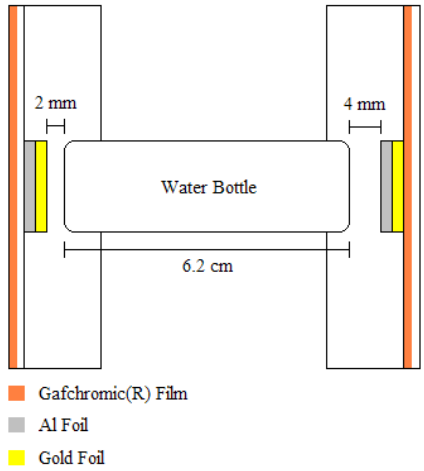

Figure 6.1.2. Target assembly used in the January 2009 RadCCORE experiment.

For the first RadCCORE experiment, the target assembly consisted of a cardboard box with three inserts placed inside. The center line through the box was placed to coincide with the beam axis so that the centers of the targets (activation foils and mouse phantom) were positioned at 0°. The cardboard box itself was placed directly in front of the gas cell. The gas cell used during the experiment was 6 cm long and made of copper with a Havar® containment foil and tantalum beam stop. The gas cell was filled with 77.6 psi (5.3 atm) of deuterium gas, which is less than the nominal operating pressure of 114.6 psi (7.8 atm), in order to produce a neutron beam having a lower energy spread. The tandem terminal voltage and analyzer magnet field were set to produce 6.990 MeV deuterons at the center of the gas cell, resulting in the production of 10.16 MeV neutrons at 0°. The energy spread of the neutron beam was ~ 320 keV at the aforementioned deuteron energy and gas cell pressure.

The end of the box closest to the gas cell and each insert possessed a 2.5 cm diameter hole which was equal in diameter to the aluminum and gold activation foils and water bottle target and was centered on the 0º beam axis. The bottle itself was made of clear plastic and was 6.2 cm in length and filled with approximately 25.5 cm^3 of water. The bottle was positioned in the target box such that the center-to-center distance between the gas cell and the water target was 13.3 cm. One of the inserts was placed near the center of the bottle to secure it. The other inserts, placed on either side of the water bottle, each held a set of activation foils, one aluminum foil and one gold foil per side. The foils were positioned inside the holes in the inserts along the 0° beam axis. Gafchromic® dosimetry film was also placed on the outside of the inserts holding the foils. Due to the finite thickness of the inserts used to hold the foils in position, there was a small air gap between the foils and the front and back sides of the water bottle target. The gap between the water bottle and foils was small, 2 mm on the front side of the water bottle (closest to the gas cell) and 4 mm on the back side. Thus, the front set of foils was located 10 cm from the center of the gas cell, while the back foils were 16.8 cm from the center of the gas cell.

Four separate runs were conducted using this setup. For the first run, the foil targets were irradiated for two hours and five minutes with an average deuteron current of 1 μA. The activated foils were then placed aside for counting and replaced with unirradiated foils; the Gafchromic® film was also replaced. A second run was then conducted with a 1/16" thick cadmium shell placed over the box for the purpose of determining its effect on shielding the target from slow neutrons ($E_n < 0.4$ eV). Natural cadmium exists as eight isotopes. Two of these isotopes, ^{113}Cd and ^{116}Cd are naturally

radioactive, with half-lives of 8.04 x 10^{15} years and 3.0 x 10^{19} years, respectively. The neutron capture cross section of most of these isotopes is on the order of a few barns; one notable exception is ^{113}Cd (natural abundance – 12.22%), which has a capture cross section of over 20,000 barns for 0.0253 eV thermal neutrons. All neutrons with energy less than 0.4 eV, the cadmium cutoff, are heavily attenuated. Above this energy, the capture cross section drops off rapidly, making cadmium an effective shield against thermal neutrons while transmitting high energy neutrons with relatively little attenuation. A cross section plot of the neutron capture reaction on ^{113}Cd is shown in **Figure 6.1.3**.

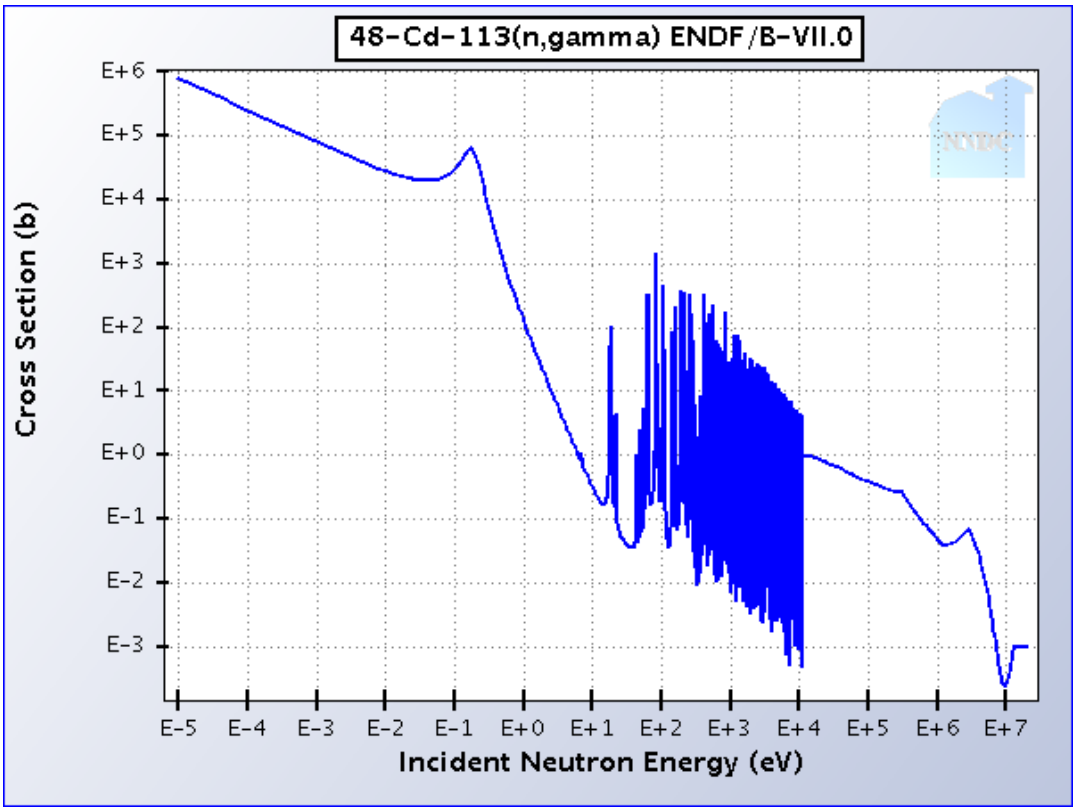

Figure 6.1.3. Cross section vs. neutron energy for the ^{113}Cd(n,γ)^{114}Cd reaction.

Subsequent to the addition of the cadmium shell, the new activation foils and water target were irradiated for two hours with an average deuteron current of 1.0 μA. For the third run, the cadmium shell was left in place and a tissue equivalent ion chamber was placed directly behind the back set of foils. No activation foils were used in this run (only film). A piece of Gafchromic® film was also added to the front surface of the box (facing the gas cell). For the fourth run, the cadmium shell was removed and activation foils were again put in place. An ion chamber was also added behind the back set of foils. The last set of foils was irradiated for one hour and fifty-five minutes at an average deuteron current of 1.3 μA. A plastic scintillator paddle (2 1/4" wide, 2 1/2" high, and 1/16" thick), positioned at 52.5 cm from the center of the gas cell along the 0º beam axis, was used to monitor the neutron flux over the course of the experiment (see **Figure 6.1.1**).

6.2 Results

The results of the first RadCCORE experiment are given in **Tables 6.2.1-6.2.8**. The foil numbers indicate the run number. The letters “F” and “B” indicate the foils in the front (closest to the gas cell) and back of the water bottle, respectively. The neutron flux and fluence were determined utilizing the methods described in Chapter 4. The fast neutron beam flux was determined using both the $^{27}Al(n,\alpha)^{24}Na$ and $^{197}Au(n,2n)^{196}Au$ reactions (see **Tables 6.2.1** and **6.2.2**). These reactions were also used to determine the attenuation of the fast neutrons in the water bottle target (see **Tables 6.2.3** and **6.2.4**). The attenuation was calculated as 1 minus the flux measured at the back of the water bottle target divided by the flux at the front position. The flux and fluence results obtained from the aluminum and gold activation foils agree well within experimental uncertainties. The

$^{197}Au(n,\gamma)^{198}Au$ reaction was used to analyze the slow neutron component of the beam. The results for the slow neutron flux measurements for the three runs with foils are given in **Table 6.2.5**. In order to determine the reduction in the slow neutron flux from the additional of the cadmium shell, the flux determined by the $^{197}Au(n,\gamma)^{198}Au$ reaction was first divided by the flux determined by either the $^{27}Al(n,\alpha)^{24}Na$ or $^{197}Au(n,2n)^{196}Au$ reaction at the same position (i.e. normalized to the fast neutron flux). The reduction in the slow neutron flux is then equal to 1 minus the normalized slow neutron flux with the cadmium shell divided by the normalized slow neutron flux without the cadmium shell. The "cadmium ratio" is equal to the normalized slow neutron flux without the cadmium shell divided by the normalized slow neutron flux with the cadmium shell measured at the same foil position. The results of the slow neutron measurements using aluminum and gold foil normalization are given in **Tables 6.2.6** and **6.2.7**, respectively. The averages of the results from both normalizations are given in **Table 6.2.8**.

Table 6.2.1. January 2009 Run – Results of the $^{27}Al(n,\alpha)^{24}Na$ Activation Foil Measurement.

Al Foils	Fast Flux (n/cm^2/s)	Fast Fluence (n/cm^2)	Error (Sys)	Error (Stat)
1F	6.565×10^6	4.924×10^{10}	± 4.8%	± 0.8%
1B	1.910×10^6	1.433×10^{10}	± 4.7%	± 0.7%
2F	5.843×10^6	4.207×10^{10}	± 4.8%	± 0.9%
2B	1.776×10^6	1.279×10^{10}	± 4.8%	± 1.0%
5F	8.475×10^6	5.847×10^{10}	± 4.8%	± 0.7%
5B	2.301×10^6	1.588×10^{10}	± 4.8%	± 0.8%

Table 6.2.2. January 2009 Run – Results of the $^{197}Au(n,2n)^{196}Au$ Activation Foil Measurement.

Au Foils	Fast Flux (n/cm^2/s)	Fast Fluence (n/cm^2)	Error (Sys)	Error (Stat)
1F	6.376×10^6	4.782×10^{10}	± 4.8%	± 0.3%
1B	1.939×10^6	1.454×10^{10}	± 4.7%	± 0.4%
2F	5.763×10^6	4.149×10^{10}	± 4.8%	± 0.3%
2B	1.850×10^6	1.332×10^{10}	± 4.8%	± 0.4%
5F	8.175×10^6	5.641×10^{10}	± 4.8%	± 0.2%
5B	2.314×10^6	1.597×10^{10}	± 4.8%	± 0.3%

Table 6.2.3. January 2009 Run – Reduction in Fast Neutron Flux Across the Water Target Determined Using Al Activation Foils.

Run	Al Front to Back Flux Reduction	Error (Sys)	Error (Stat)
1	70.9%	± 4.7	± 0.8
2	69.6%	± 4.6	± 1.0
5	72.8%	± 4.8	± 0.8
Average	71.1%	± 2.7	± 0.5

Table 6.2.4. January 2009 Run – Reduction in Fast Neutron Flux Across the Water Target Determined Using Gold Activation Foils.

Run	Au Front to Back Flux Reduction	Error (Sys)	Error (Stat)
1	69.6%	± 4.6	± 0.4
2	67.9%	± 4.5	± 0.3
5	71.7%	± 4.8	± 0.3
Average	69.7%	± 2.7	± 0.2

Table 6.2.5. January 2009 Run – Results of the $^{197}Au(n,\gamma)^{198}Au$ Activation Foil Measurement.

Au Foils	Slow Flux (n/cm^2/s) (Relative)	Slow Fluence (n/cm^2) (Relative)	Error (Sys)	Error (Stat)
1F	6.376×10^3	4.782×10^7	± 4.8%	± 0.8%
1B	4.396×10^3	3.297×10^7	± 4.7%	± 0.6%
2F	4.891×10^3	3.521×10^7	± 4.8%	± 0.8%
2B	2.915×10^3	2.099×10^7	± 4.8%	± 0.7%
5F	5.367×10^3	3.703×10^7	± 4.8%	± 0.7%
5B	5.009×10^3	3.456×10^7	± 4.8%	± 0.5%

Table 6.2.6. Slow Neutron Flux Reduction by the Cd Shell Based on Al Activation Foil Normalization.

Position	Al Normalization	Error (Sys)	Error (Stat)	Cd Ratio
Front	13.8%	± 0.2	± 0.2	1.16
Back	28.7%	± 0.5	± 0.4	1.40

Table 6.2.7. Slow Neutron Flux Reduction by the Cd Shell Based on Au Activation Foil Normalization.

Position	Au Normalization	Error (Sys)	Error (Stat)	Cd Ratio
Front	15.1%	± 0.2	± 0.2	1.18
Back	30.5%	± 0.5	± 0.3	1.44

Table 6.2.8. Average (Al and Au foils) of Slow Neutron Flux Reduction by the Cd Shell.

Position	Total Average	Error (Sys)	Error (Stat)	Cd Ratio
Front	14.5%	± 0.2	± 0.1	1.17
Back	29.6%	± 0.3	± 0.3	1.42

6.3 Discussion and Summary

The first RadCCORE experiment established the effectiveness of using aluminum and gold activation foils as passive monitors of the fast and thermal neutron flux, respectively. Using a 6 cm gas cell filled with 5.3 atm of deuterium gas and a deuteron current of 1 μA, fast neutron fluxes up to 6.6 x 10^6 n/(cm^2 s) were achieved at 10 cm from the center of the gas cell. The neutron flux determined from the independent aluminum and gold foil measurements were found to be in very close agreement (<5% difference for all measurements). The reduction in fast neutron flux from the front to the back of the water bottle target, averaged over all results from the aluminum and gold activation measurements, was determined to be approximately 70.4%. This reduction was due to the combined effects of neutron attenuation in the water bottle target and distance dependent flux fall-off. The slow neutron measurement was intrinsically relative since the exact energy distribution of the thermal neutrons at the target position was unknown. The relative slow neutron flux values previously listed were calculated assuming a $^{197}Au(n,\gamma)^{198}Au$ reaction cross section of 100 barns (the approximate cross section for thermal neutrons). The relative flux values from the gold foil measurement were then normalized to the fast neutron flux at the same foil position measured using the aluminum and gold foils, respectively, in order to accurately determine the slow neutron flux reduction due to the addition of the cadmium shell. The reduction in the slow neutron flux, averaged over the results from the aluminum and gold normalization, was found to

be 14.5% at the front foil position, and 29.6% at the back foil position, implying cadmium ratios of 1.17 and 1.42, respectively.

One half millimeter of natural cadmium is sufficient to stop greater than 99% of all neutrons with energy less than 0.4 eV. The relatively low drop in the measured slow neutron flux with the addition of the cadmium shell implies the majority of the background at the target position is comprised of neutrons with energies greater than 0.4 eV where the cadmium cross section is significantly lower (see **Figure 6.1.3**). This conjecture is supported by the greater cadmium ratio observed at the back foil position. In the absence of the cadmium shell, intermediate energy neutrons from the gas cell would make a moderate contribution to the activation of the front gold foil. However, many of the intermediate energy neutrons would be thermalized while passing through the water bottle target and subsequently make a much greater contribution to the activation of the back foil. With the addition of the cadmium shell, and subsequent moderate reduction in the intermediate energy neutron flux, the relative flux reduction at the back position would be expected to be slightly greater than at the front position, consistent with observation.

However, it should be noted that the cadmium shell used (1/16") was much thicker than what is typically employed for thermal neutron shielding. The average ^{nat}Cd(n,tot) cross section at 10.16 MeV neutron energy is about 4.6 barns, resulting in ~ 3.3% total attenuation of the fast neutron beam, potentially distorting the results of the measurement.

7. April 2009 RadCCORE Experiment

A new target holder designed to hold six test tubes in symmetric off-axis positions was used during the second RadCCORE experiment. The primary objectives during this experiment were: (1) to measure the attenuation of fast neutrons through water bottle phantoms placed at 0° and in an off-axis position and (2) to measure the difference in the fast neutron fluence at an off-axis position of the new target holder compared to the fast neutron fluence at the center (i.e. 0°). A description of the experiment, techniques, and results for the April 2009 experiment are presented in this chapter.

7.1 Experiment Setup and Description

An annotated photograph of the test tube and water bottle phantom can be seen in **Figure 7.1.1**. The target holder assembly is shown in **Figure 7.2.2**.

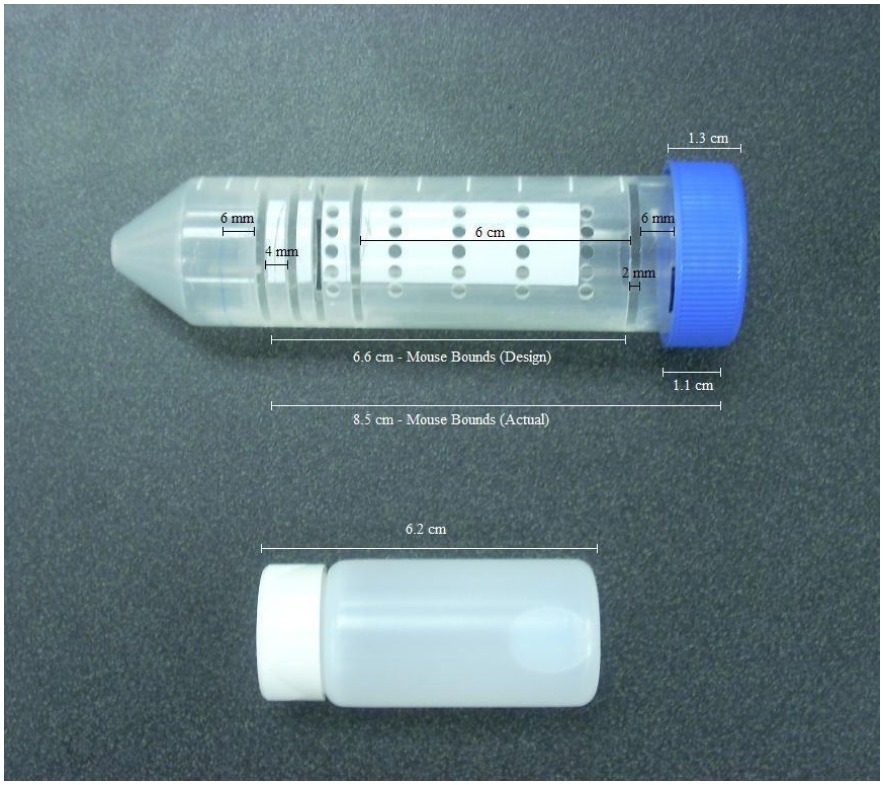

Figure 7.1.1. Test tube and water bottle target.

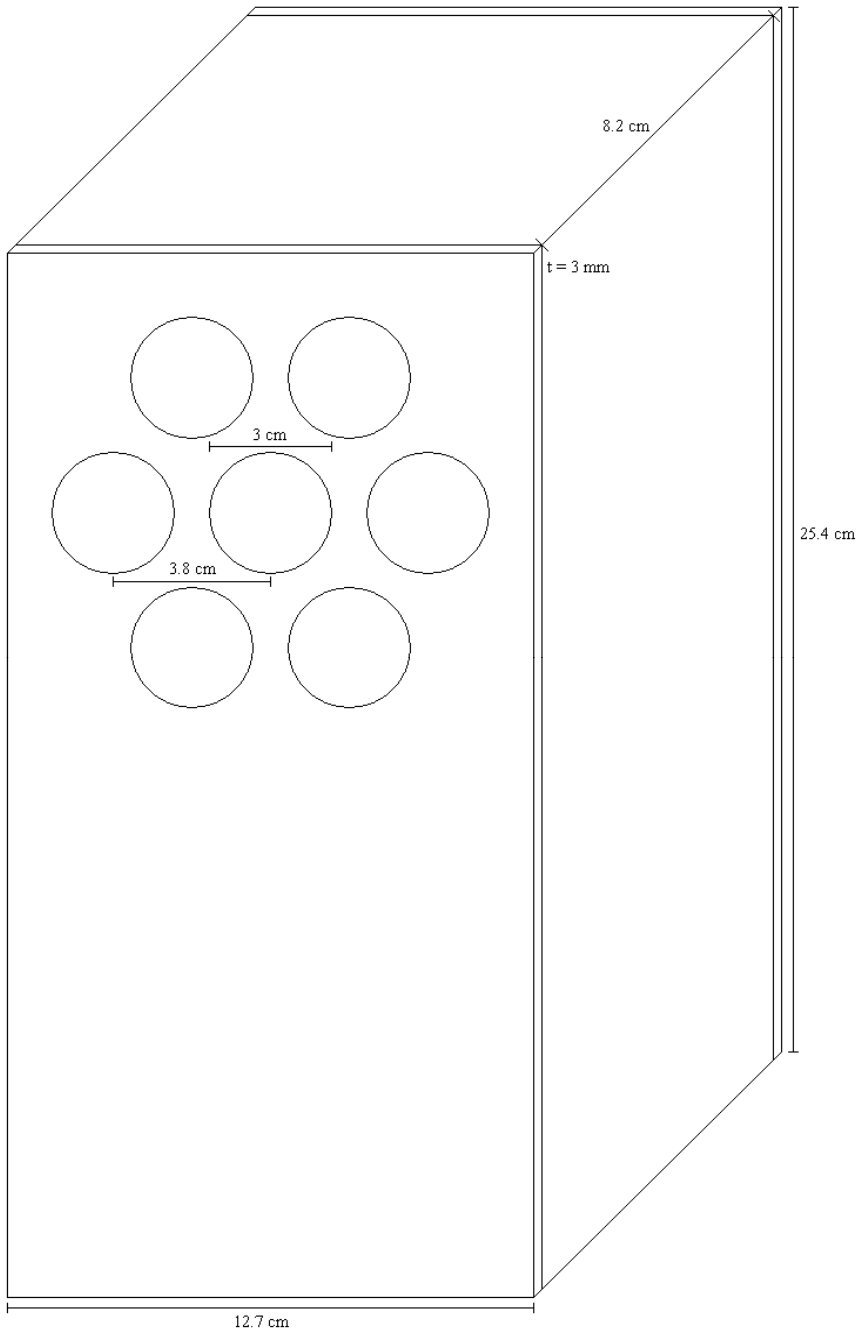

Figure 7.1.2. Mouse target holder diagram.

The new holder was comprised of two parallel plastic plates, 12.7 cm wide, 25.4 cm high, 3 mm thick, and spaced 7.6 cm apart. The plates had seven 3 cm diameter holes drilled through them, with six peripheral holes positioned symmetrically around a central hole aligned with the 0º beam axis such that the center to center distance between each peripheral hole and the central hole was 3.8 cm. The holder was suspended on four metal rods that allowed the height of the apparatus to be adjusted. The bottoms of the rods were attached to an actuator that would allow the holder to be rotated 360°. The rotation feature was not used during the second RadCCORE experiment.

Inside the target holder were placed two plastic test tubes, 10.4 cm in length with diameter equal to that of the holes in the target holder. One test tube was placed in the central position (along the 0º beam axis), while the other was placed in the middle-right position (with respect to the beam direction) of the holder. Water bottle targets of identical dimensions as used in the first experiment were placed in the center of each test tube, and aluminum activation foils were placed on either side of the water target. The foils were mounted on 1.5 mm thick plastic inserts that fit within slots cut on either side of the water bottle. These inserts, while not strictly necessary in the second experiment, served two main purposes: 1) to immobilize the intended live mouse targets to be used in the third experiment and 2) to protect the activations foils from physical damage by a live mouse.

The same 6 cm gas cell was used as in the first RadCCORE experiment, but the deuterium pressure was increased to 7.8 atm in order to achieve a higher neutron flux. The tandem terminal voltage and analyzer magnet field were set to produce 6.823 MeV deuterons at the center of the gas cell, resulting in the production of 10.00 MeV neutrons

at 0°. The increased mass thickness of the gas caused the energy spread of the neutrons produced to increase to ~ 480 keV. The water bottle in the central position of the target holder was placed 16.5 cm from the gas cell (center to center). The front activation foil in the center position was 13 cm from the center of the gas cell, while the back foil was 20 cm from the center of the gas cell. The water bottle in the side position was 16.9 cm from the gas cell (center to center). The front activation foil in the side position was 13.5 cm from the center of gas cell, while the back foil was 20.4 cm from the center of the gas cell.

As previously discussed, the neutron energy at off-axis positions is lower than the nominal value along the 0° axis. The angles with respect to the 0° axis of the centers of the side front and back activation foils, and the center of the side water bottle target are listed along with the corresponding neutron energy at each angle in **Table 7.1.1**.

Table 7.1.1. April 2009 Run – Setup Data.

	Angle (degrees)	Neutron Energy (MeV)
Side Front Foil	16.29	9.671
Side Back Foil	10.76	9.855
Water Bottle (Center)	12.97	9.789

During the single run performed for the second RadCCORE experiment, the target setup was irradiated for one hour and fifty-seven minutes at an average deuteron current of 1.305 μA.

7.2 Results

The results of the second RadCCORE experiment are given in **Tables 7.2.1-7.2.3**. The fast neutron flux and fluence (**Table 7.2.1**) and reduction in fast neutron fluence across the water target (**Table 7.2.2**) were determined in the same manner as in the first

RadCCORE experiment. The reduction in the measured fast neutron flux for the front and back foils, respectively, at the off-axis position relative to that measured at 0º was calculated as 1 minus the fast neutron flux measured at the side position divided by the flux measured at the center position (see **Table 7.2.3**).

Table 7.2.1. April 2009 Run – Results of the $^{27}Al(n,\alpha)^{24}Na$ Activation Foil Measurement.

Al Foils	Fast Flux (n/cm^2/s)	Fast Fluence (n/cm^2)	Error (Sys)	Error (Stat)
Center Front	1.012×10^7	7.106×10^{10}	± 4.8%	± 0.4%
Center Back	1.429×10^6	1.003×10^{10}	± 4.8%	± 0.8%
Side Front	5.041×10^6	3.539×10^{10}	± 4.8%	± 0.7%
Side Back	1.309×10^6	9.188×10^9	± 4.8%	± 0.8%

Table 7.2.2. April 2009 – Reduction in Fast Neutron Flux Across the Water Target Determined Using Al Activation Foils.

Foil Position	Flux Reduction	Error (Sys)	Error (Stat)
Center	85.9%	± 0.2	± 0.8
Side	74.0%	± 0.1	± 0.8

Table 7.2.3. Reduction in Fast Neutron Flux at Off-Axis Position Compared to 0º.

Foil Position	Flux Reduction	Error (Sys)	Error (Stat)
Front	50.2%	± 3.4	± 0.4
Back	8.4%	± 0.6	± 0.1

7.3 Discussion and Summary

The higher beam current and gas cell pressure used during the second RadCCORE experiment allowed a 10 MeV neutron flux of 1×10^7 n/(cm^2 s) to be achieved at 13 cm from the center of the gas cell along the 0° axis. A larger magnitude reduction in the measured neutron flux through the central water bottle target was observed in comparison to the first RadCCORE experiment (85.9% vs. 70.4%). This

difference is a result of the different target distance used in the second RadCCORE experiment; the actual attenuation by the water bottle target should be the same since the target is identical to that used in the first RadCCORE experiment and the monitor foils were placed in the same positions with respect to the bottle. The fast neutron flux reduction through the water bottle target was observed to be less at the side position than at 0º due to lower target attenuation as a result of the neutron beam irradiating the target at an angle as opposed to head on. Knowledge of the differences in the neutron flux at the side target position in comparison to 0° was critical for planning the first mouse activation run in the third RadCCORE experiment in May 2009. In the absence of attenuation, the drop off in measured neutron flux at the side front foil position from that measured at 0° was found to be 50.2%. This value is in good agreement with the 56.1% decrease in flux predicted from the difference in the differential cross section for the $^{2}H(d,n)^{3}He$ reaction at 16.29° compared to 0°. It was also discovered during this run that the back target foils in the center and side positions were very evenly irradiated. The measured flux at the back off-axis position was 91.6% the corresponding flux at the center back position.

8. May 2009 RadCCORE Experiment

The third RadCCORE experiment, conducted in May 2009, had the following objectives: (1) use an off-axis neutron monitor to estimate the dose to mouse targets in real time and (2) irradiate two sets of live mouse targets with goal doses of 50 and 200 cGy, respectively. A description of the experiment, techniques, and results for the May 2009 experiment are presented in this chapter.

8.1 Experiment Setup and Description

For the third RadCCORE experiment, two sets of live mice were irradiated. The mice were placed in the peripheral positions of the target holder within the same types of test tubes as used for the second experiment. The gas cell was filled with 7.8 atm of deuterium gas and the tandem terminal voltage and analyzer magnet field were set to produce 6.823 MeV deuterons at the center of the gas cell, resulting in the production of 10.00 MeV neutrons at 0°. The energy spread of the neutron beam was ~ 480 keV. To monitor the neutron flux during the experiment, a 2" liquid scintillation detector was placed 333.4 cm from the center of the gas cell at a 60° angle with respect to the beam axis. Using the results from the second experiment, the neutron fluence incident upon the front face of the target holder at the off-axis position was estimated based on the live count rate measured from the 60° neutron monitor. The details of this calculation can be found in **Appendix C**.

The first set of mice was irradiated until an estimated dose of 200 cGy had been delivered. A second set of mice in the same target positions was also irradiated with an estimated dose of 50 cGy. For both runs, the mice were inserted into the test tubes so that their heads faced the tip of the tubes, while their tails were adjacent to the cap. The target

holder was positioned such that the distance between the center of the gas cell and the center of the target holder was 15 cm. The target holder was rotated 180° half-way through irradiation (equal neutron counts in the in the 60° monitor) in order to deliver a more uniform dose to the targets. The cap sides of the targets (mouse tails) were irradiated first for the 200 cGy run, while the tip sides of the targets (mouse heads) were irradiated first for the 50 cGy run. Aluminum activation foils were used to determine the fast neutron fluence incident upon the head and tail ends of the mice in the center left and center right (with respect to the beam direction) target holder positions. The foil numbers and starting / end positions for each run are shown in **Figure 8.1.1**. The letters “F” and “B” next to the foil numbers indicate the position of the foil on the test tube, “F” for the front (cap of the test tube / mouse tail) and “B” for the back (tip of the test tube / mouse head), respectively.

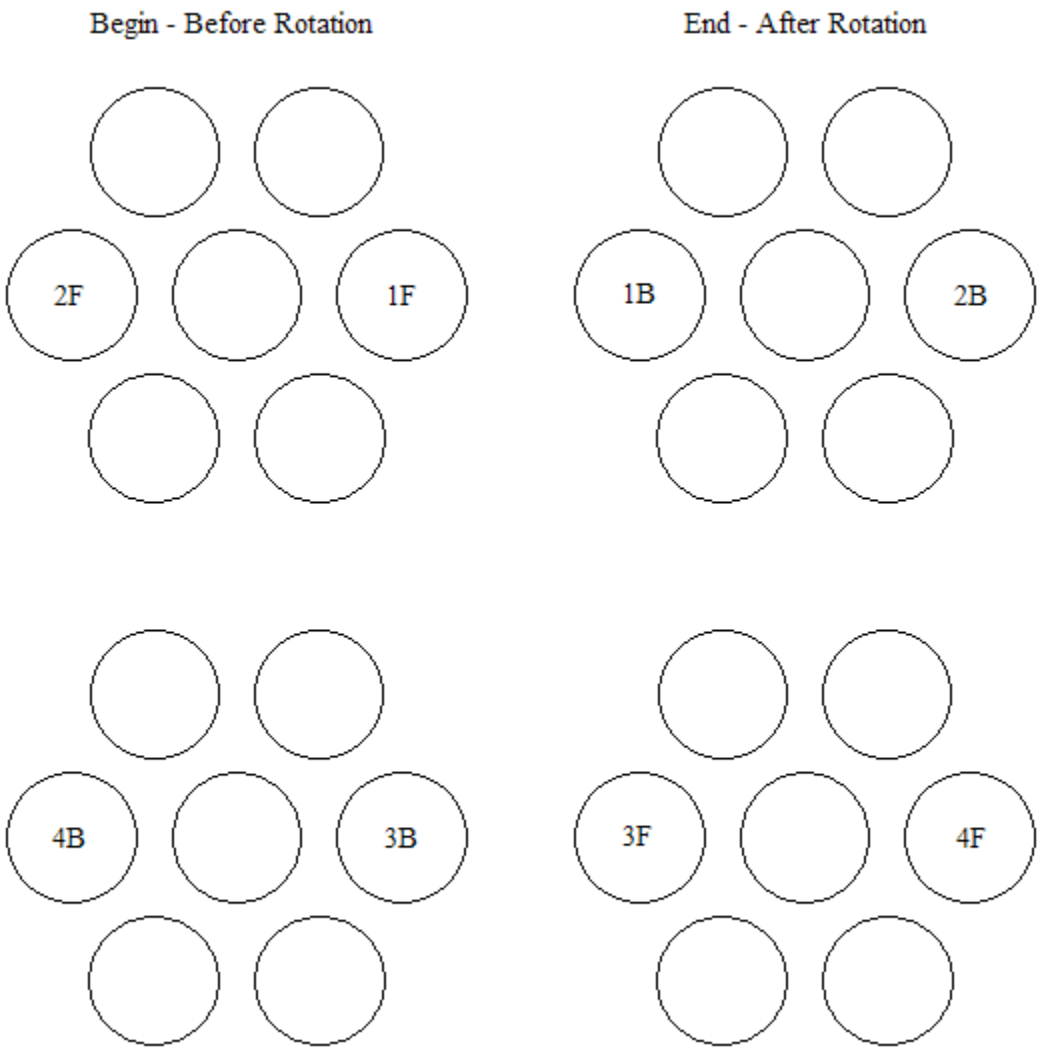

Figure 8.1.1. May 2009 activation foil starting and stopping positions.

In the original setup configuration for the experiment, the mouse centers were exactly 15.5 cm from the center of the gas cell, before and after rotation. The activation foil nearest the gas cell was 12.1 cm from the center of the cell, while the foil on the opposite side was 18.9 cm from the center of the gas cell, regardless of the orientation of the test tube itself (tip or cap side facing the gas cell). However, it was discovered the live

mice were longer than the water bottle phantoms used in the previous experiments. To compensate for this unexpected development, the insert nearest the cap of the test tube was removed and the foil originally attached to this insert was placed on the test tube cap itself. As a result of this change, the head and tail foil positions and mouse center were no longer symmetric with respect to rotation. The original and actual mouse bounds can be seen in **Figure 7.1.1**.

Since the target holder was rotated midway through each of the two runs, there were two positions for each foil, rotated "toward" the gas cell (i.e. closer distance), and rotated "away" from the gas cell. Likewise, the mouse center distance from the center of the gas cell varied according to which side (cap or tip) of the test tube was rotated toward the gas cell at that time. **Table 8.1.1** lists the foil and mouse center distances (in cm), the lab angle with respect to the center of the gas cell (in degrees), the neutron energy at these angles (in MeV), and the corresponding neutron kerma factors for muscle tissue (in cGy cm^2/n). The rotation column indicates the position with respect to the gas cell.

Table 8.1.1. May 2009 Run – Setup Data.

	Rotation	Distance	Angle	Energy (MeV)	KF (cGy cm^2/n)
Cap Foil (Tail)	Toward	10.3	21.60	9.431	5.570×10^{-9}
Cap Foil (Tail)	Away	20.8	10.55	9.861	5.692×10^{-9}
Tip Foil (Head)	Toward	12.1	18.29	9.588	5.616×10^{-9}
Tip Foil (Head)	Away	18.9	11.61	9.832	5.686×10^{-9}
Mouse (Center)	Toward	14.6	15.13	9.716	5.655×10^{-9}
Mouse (Center)	Away	16.4	13.40	9.776	5.673×10^{-9}

The average neutron energy for the cap (tail) foils was found to be 9.646 MeV, while the average for the tip (head) foils was 9.710 MeV. The average neutron energy at the position of the mouse centers was 9.746 MeV. With respect to the cap foils (tail), the cross section for the $^{27}Al(n,\alpha)^{24}Na$ reaction increases by 7.9% from 9.431 MeV to 9.861

MeV (cap tail). Likewise, for the tip foils (head), the cross section increases by 3.9% between 9.588 MeV and 9.832 MeV. These increases are small enough such that ± 10% dose measurements (an initial goal of the RadCCORE collaboration) can still be achieved.

When calculating the neutron flux incident on the two sides of the mouse, the average $^{27}Al(n,\alpha)^{24}Na$ cross section for each activation foil was used. For the cap foils, the cross section value used was the average between the value at 9.431 MeV and the value at 9.861 MeV. The average cross section for the tip foil was calculated in like manner. In order to calculate the dose to tissue at each foil position, the neutron fluence values calculated using the above methodology were multiplied by the average neutron kerma factors. The average neutron kerma factor for each foil was calculated the same way as the average activation cross section. Since neutron kerma factors for mouse tissue specifically were not available, kerma factors for adult muscle tissue were used in the calculations. The kerma factors at the relevant neutron energies were calculated from linear interpolation of the tabulated values found in ICRU Report 46[1].

8.2 Results

The results of the third RadCCORE experiment are given in **Tables 8.2.1** and **8.2.2**. Flux and fluence values were calculated the same as in the first and second RadCCORE experiments. Dose values were determined using the relevant neutron kerma factors for each foil given in **Table 8.1.1**.

[1] ICRU Report 46 (pg. 175)

Table 8.2.1. May 2009 Run – 200 cGy Irradiation Data.

Foil	Flux (n/cm^2/s)	Fluence (n/cm^2)	Dose (cGy)	Error (Sys)	Error (Stat)
1F (Tail)	3.664 x 10^6	3.408 x 10^{10}	192	4.7%	2.1%
1B (Head)	2.874 x 10^6	2.672 x 10^{10}	151	4.7%	2.2%
2F (Tail)	2.357 x 10^6	2.192 x 10^{10}	123	4.7%	2.9%
2B (Head)	3.713 x 10^6	3.453 x 10^{10}	195	4.7%	1.2%

Table 8.2.2. May 2009 Run – 50 cGy Irradiation Data.

Foil	Flux (n/cm^2/s)	Fluence (n/cm^2)	Dose (cGy)	Error (Sys)	Error (Stat)
3F (Tail)	3.263 x 10^6	5.874 x 10^9	33.1	5.7%	3.6%
3B (Head)	4.943 x 10^6	8.898 x 10^9	50.3	5.7%	2.7%
4F (Tail)	4.300 x 10^6	7.740 x 10^9	43.6	5.7%	2.7%
4B (Head)	3.861 x 10^6	6.627 x 10^9	37.4	5.7%	2.8%

The following additional systematic uncertainties may be added to those cited above to account for variance in the Al(n,α) cross section that results from the change in the neutron energy incident upon the foils due to rotation:

Cap Foils (F): 3.9%

Tip Foils (B): 2.0%

8.3 Discussion and Summary

A tissue dose close to the target value was achieved on at least one side of each mouse irradiated, demonstrating the feasibility of using an off-axis neutron monitor for real time dose estimation. All foils within each set should have been irradiated evenly, but a consistent neutron flux asymmetry was discovered between the left and right sides of the target holder. The target foils on the left side (with respect to the beam direction) of

the gas cell were consistently irradiated at a lower neutron flux than those on the right side for both the 200 cGy and 50 cGy runs (see **Figure 8.1.1**).

There are several possible explanations for the measured asymmetry. The asymmetry could be partially due to beam steering effects (i.e. the deuteron beam entering the gas cell at an angle instead of head on). However, given the small diameter of the gas cell, it is unlikely beam steering effects alone could account for the magnitude of the flux difference detected. A stronger possibility is that the target setup itself was slightly off center. A telescope in the back of the TUNL Time-of-Flight room is used to determine the 0° line from the gas cell. If the telescope was slightly misaligned, the target holder setup could have been centered at an off-axis angle. The asymmetry may also have been the result of a combination of misalignment and beam steering effects.

9. July 2009 RadCCORE Experiment

The fourth RadCCORE experiment, conducted in July 2009, had the following objectives: (1) achieve faster dose delivery using a LN_2 cooled gas cell, (2) use a 0º plastic scintillator paddle to estimate the dose to mouse targets in real time and (3) irradiate nine sets of live mouse targets, three sets each with goal doses of 50, 200 cGy, and 500 cGy, respectively. A description of the experiment, techniques, and results for the July 2009 experiment are presented in this chapter.

9.1 Experiment Setup and Description

For the fourth RadCCORE experiment performed in July 2009, the pre-existing target holder was used in conjunction with a new liquid nitrogen cooled gas cell (**Figure 9.1.1**). Using liquid nitrogen (boiling point = 77 K) cooling allowed the gas cell to be filled with more deuterium gas while keeping the pressure at 7.8 atm. The greater number of deuterium atoms available for the $^{2}H(d,n)^{3}He$ reaction in turn allowed higher neutron fluxes to be achieved with the same beam currents used in the previous experiments. Thus, a greater target dose could be delivered in a shorter time. However, the greater effective gas thickness also resulted in a larger energy spread of the neutrons created along the length of the gas cell. A small leak in the gas cell caused the 0° neutron energy to increase marginally over the course of each run. As a consequence, the gas cell pressure was “topped off” before each new set of mice was irradiated. The average gas cell pressure over the course of the runs was 102.5 psi (7.0 atm) at 77 K corresponding to 390 psi (26.5 atm) at room temperature (293 K). At this pressure, 7.042 MeV deuterons were produced at the center of the gas cell leading to the production of 10.21 MeV neutrons at 0°. The energy spread of the neutrons across the length of the gas cell (2.02")

was +1.24 MeV / - 1.47 MeV. The average deuteron current for the fourth RadCCORE experiment was 1.43 μA.

Before loading the live mouse targets, a preliminary run was conducted to calibrate the scintillator paddle used for neutron flux monitoring. The details of this calculation can be found in **Appendix D**.

Subsequent to the calibration run, nine sets of six mice each (all positioned in the peripheral holes of the target holder) were irradiated at target doses of 50 cGy, 200 cGy, and 500 cGy, respectively. Three sets were irradiated at each target dose. Before mice were loaded into the target holder, the table on which the target holder and scintillator paddle were positioned was moved forward so that the distance between the center of the gas cell and the center of the target holder was 20 cm (i.e. the activation foil distance in the calibration run). Since all the mice were positioned symmetrically around the center position of the target holder, only a single foil set (one foil in front of and one behind a single mouse) was used to monitor the fluence incident upon the six mice irradiated during each run. **Table 9.1.1** lists the foil and mouse center distances (in cm), the lab angle with respect to the center of the gas cell (in degrees), the neutron energy at these angles (in MeV), and the corresponding neutron kerma factors for muscle tissue (in cGy cm^2/n).

Table 9.1.1. July 2009 Run – Setup Data.

	Rotation	Distance	Angle	Energy (MeV)	KF (cGy cm^2/n)
Cap Foil (Tail)	Toward	15.1	14.59	9.937	5.704×10^9
Cap Foil (Tail)	Away	25.7	8.51	10.117	5.743×10^9
Tip Foil (Head)	Toward	16.9	12.97	9.993	5.719×10^9
Tip Foil (Head)	Away	23.8	9.19	10.101	5.740×10^9
Mouse (Center)	Toward	19.4	11.28	10.046	5.729×10^9
Mouse (Center)	Away	21.3	10.28	10.073	5.735×10^9

As in the third RadCCORE experiment, the target holder was rotated 180° at the midpoint of each run in order to achieve more uniform irradiation of the targets. The average neutron energy for the cap (tail) foil was 10.027 MeV, while the average for the tip (head) foil was 10.047 MeV. The average neutron energy at the position of the mouse center was 10.060 MeV. For the cap foil (tail), the cross section for the (n,α) reaction increases by 3.2% from 9.937 MeV to 10.117 MeV (cap tail). For the tip foil (head), the cross section increases by 2.0% between 9.993 MeV and 10.101 MeV. The average neutron flux/fluence and kerma factors for each foil position were calculated in the same manner as in the third experiment. The foil position was varied during the fourth RadCCORE experiment to determine if the asymmetry measured between the middle-left and middle-right off-axis positions in the third experiment was still present.

The starting and stopping positions of the irradiation foils for each set of runs are shown in **Figure 9.1.2**. In each instance, the tip ("B") foils (corresponding to the mouse tail) were irradiated first. The left side letter and number indicate the foil number and position (F – Test Tube Cap / Mouse Tail, B – Test Tube Tip / Mouse Head), while the last letter shows the position of each foil at the beginning (B) and end (E) (i.e. after rotation) of irradiation.

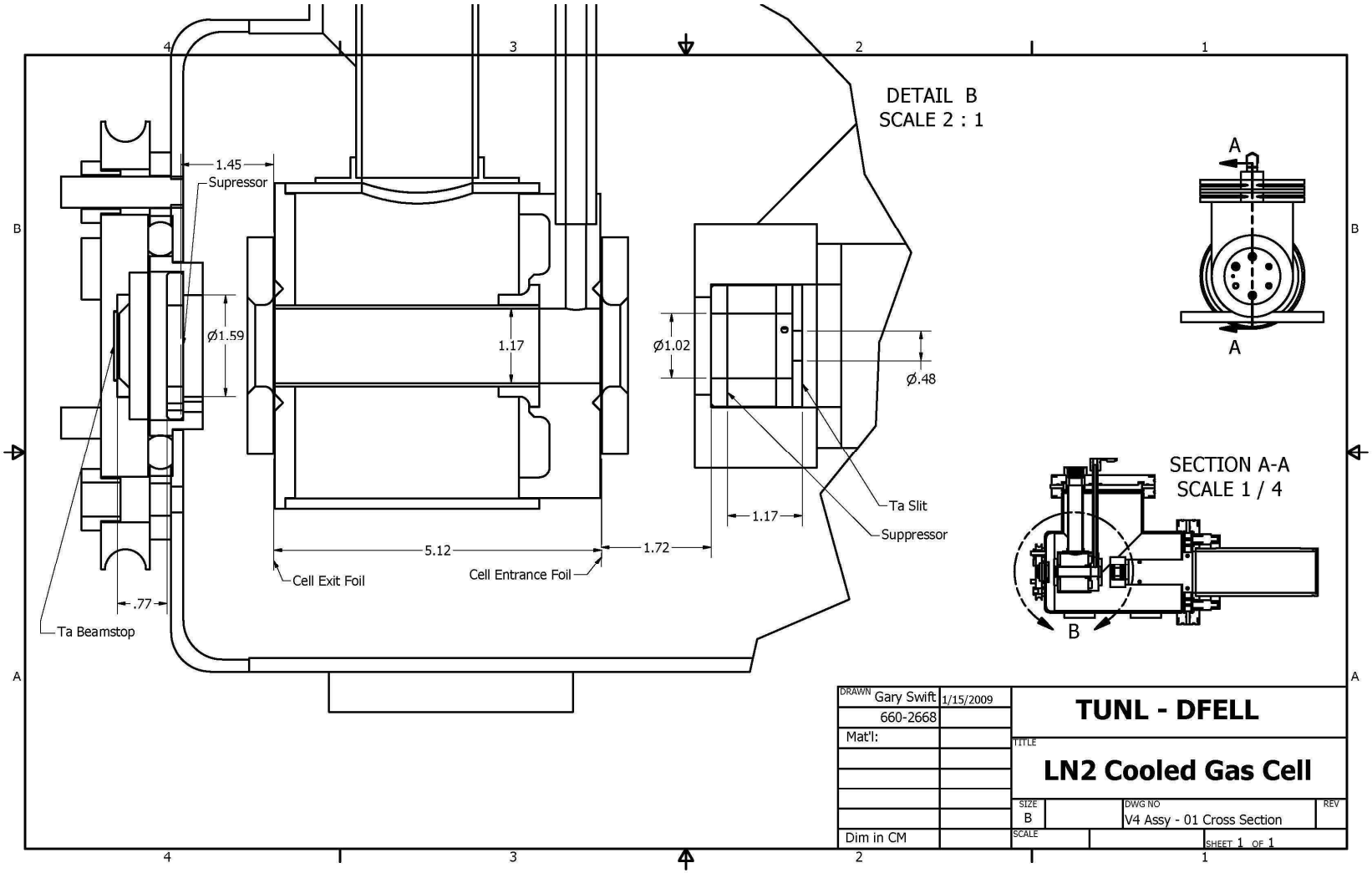

Figure 9.1.1. Schematic diagram of the LN_2 gas cell designed for the fourth RadCCORE experiment.

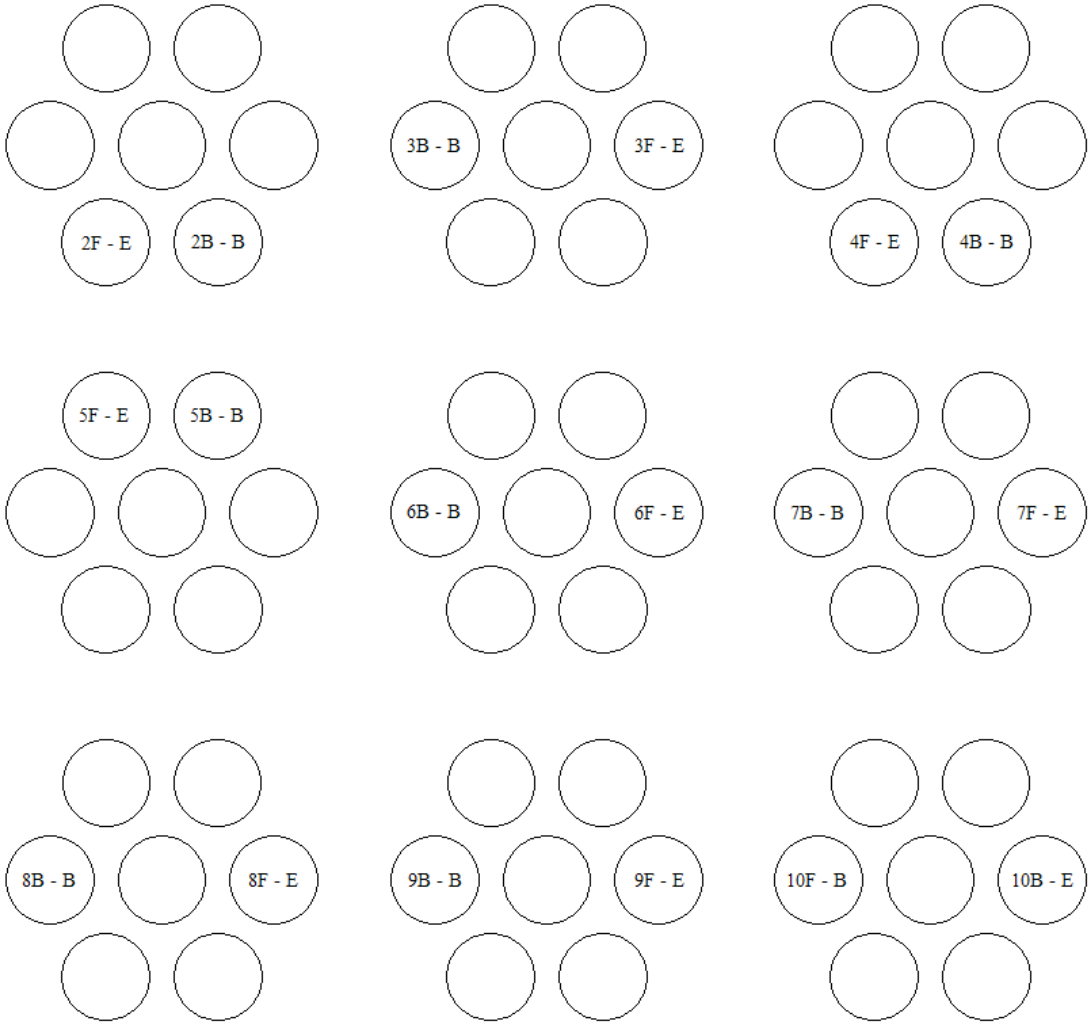

Figure 9.1.2. July 2009 activation foil starting and stopping positions.

9.2 Results

The results of the third RadCCORE experiment are given in **Tables 9.2.1** and **9.2.2**. Flux and fluence values were calculated the same as in the first, second, and third RadCCORE experiments. Dose values were determined using the relevant neutron kerma factors for each foil given in **Table 9.1.1**. In the following data, the foil number indicates the run number. The front foils (F) were in the cap position (mouse tail), while the back foils (B) were in the tip position (mouse head) for all runs except the last in which the front and back foil positions were accidentally reversed. The tip side was irradiated first for all runs. The asymmetry between the left and right side foil positions given in **Table 9.2.1** was calculated as the flux value for the right side foil divided by the flux value for the left side foil, where the "left" and "right" side foils are defined as shown in **Figure 9.1.2**. The letter next to the asymmetry values (i.e. T, B, M) indicates the foil positions in the target holder (i.e. top, bottom, middle) (see **Figure 9.1.2**). The percent goal doses in **Table 9.2.2** were calculated as the actual dose determined via the foil activation technique divided by the goal dose.

Table 9.2.1. July 2009 Run – Results of the $^{27}Al(n,\alpha)^{24}Na$ Activation Measurement.

Foil	Flux (n/cm^2/s)	Fluence (n/cm^2)	Error (Sys)	Error (Stat)	L/R Assym.
2F	3.900×10^6	5.995×10^9	3.2%	1.0%	1.17 (B)
2B	4.577×10^6	7.035×10^9	3.2%	1.7%	
3F	8.111×10^6	1.138×10^{10}	3.2%	0.9%	1.34 (M)
3B	6.074×10^6	8.522×10^9	4.7%	1.0%	
4F	4.571×10^6	6.999×10^9	3.2%	1.0%	1.00 (B)
4B	4.591×10^6	7.029×10^9	4.7%	0.9%	
5F	6.585×10^6	3.933×10^{10}	3.2%	0.5%	1.06 (T)
5B	6.972×10^6	4.164×10^{10}	4.7%	0.5%	
6F	6.248×10^6	1.035×10^{11}	3.2%	0.3%	1.38 (M)
6B	4.542×10^6	7.523×10^{10}	4.7%	0.3%	
7F	6.923×10^6	4.594×10^{10}	3.2%	0.5%	1.37 (M)
7B	5.038×10^6	3.343×10^{10}	4.7%	0.5%	
8F	6.221×10^6	1.013×10^{11}	3.2%	0.3%	-
8B*	2.969×10^6	4.836×10^{10}	4.7%	0.4%	
9F	8.813×10^6	4.745×10^{10}	3.2%	0.4%	1.41 (M)
9B	6.234×10^6	3.356×10^{10}	4.7%	0.5%	
10F	5.989×10^6	8.810×10^{10}	3.2%	0.3%	1.19 (M)
10B	7.120×10^6	1.047×10^{11}	4.7%	0.3%	

Table 9.2.2. July 2009 Run – Calculated Dose to Target

Foil	Goal (cGy)	Actual (cGy)	Error (Sys)	Error (Stat)	% Goal
2F	50	34.3	1.1	0.3	0.69
2B	50	40.3	1.3	0.7	0.81
3F	50	65.1	2.1	0.6	1.30
3B	50	48.8	2.3	0.5	0.98
4F	50	40.1	1.3	0.4	0.80
4B	50	40.3	1.9	0.4	0.81
5F	200	225.2	7.4	1.2	1.13
5B	200	238.6	11.3	1.2	1.19
6F	500	592.4	19.4	1.8	1.18
6B	500	431.0	20.3	1.5	0.86
7F	200	263.0	8.6	1.2	1.32
7B	200	191.5	9.0	1.0	0.96
8F	500	580.1	19.0	1.9	1.16
8B	500	277.1	13.0	1.2	0.55
9F	200	271.7	8.9	1.2	1.36
9B	200	192.3	9.0	0.9	0.96
10F	500	504.8	16.5	1.8	1.01
10B	500	599.7	28.3	1.8	1.20

*Note: The mouse kicked out the tab holding the activation foil during the course of this run resulting in a significantly lower measured neutron flux.

The following additional systematic uncertainties may be added to those cited in **Tables 9.2.1** and **9.2.2** to account for variance in the Al(n,α) cross section that results from the change in incident neutron energy due to rotation:

Cap Foils (F): 1.6%

Tip Foils (B): 1.0%

9.3 Discussion and Summary

The average dose to target over all runs was 104% of the target dose with a standard deviation of 21%. An equal number of targets foils were found to be over-irradiated as under-irradiated. As in the third RadCCORE experiment, a prominent left-right asymmetry was observed between the activation foils. When the activation foils were placed in the middle left or right target holder positions, the foil that was irradiated on the right side position (with respect to the beam direction), either before or after rotation, was found to have been exposed to a significantly higher neutron flux than the corresponding foil on the left side. This effect was also observed when the activation foils were placed in the top and bottom target holder positions, however, to a much lesser extent. The foils placed in the bottom target holder position (i.e. foil sets 2 and 4, both 50 cGy runs) were observed to be under-irradiated by approximately 25% (average), while those placed in the top position (i.e. foil set 5 – 200 cGy run) were found to be over-irradiated by about 16.5% (average). The combination of these observed effects implies that the target setup was most likely misaligned relative to the gas cell during the third and fourth RadCCORE experiments. The additional information determined through

varying the monitor foil positions in the fourth RadCCORE experiment suggests the center of the target setup was slightly low with respect to the gas cell height and also shifted to the left (with respect to beam direction), giving a higher neutron flux at the right side positions and top half of the target holder. As it is unlikely that the target holder setup was consistently misaligned in the same manner for both the third and fourth RadCCORE experiments, the mostly likely explanation is a misalignment of the telescope at the back of the Time-of-Flight room that was used to determine the 0° beam axis.

10. RadCCORE Summary

10.1 Final Observations

The 2009 RadCCORE project marked TUNL's first foray into small animal irradiation experiments. For a laboratory that has traditionally engaged primarily in fundamental nuclear physics research, developing the methodology to accurately deliver pre-determined uniform doses of neutron radiation to live targets was a unique challenge. Not unexpectedly, several problems arose along the way that complicated the target dose delivery and data analysis.

The main hurdle to overcome was the issue of uniform dose delivery across multiple extended targets. To this end, a target holder was constructed allowing seven targets to be irradiated simultaneously, one in a central position and six along the periphery. The holder was designed to be remotely rotated 180° mid-irradiation to allow for more uniform dose delivery. Real time monitoring of the neutron flux using liquid and plastic scintillation detectors was used to estimate the dose-rate at the target position. Monitor foils were also placed at the front and back of the targets for a more precise determination of the actual incident neutron dose to the mouse targets.

In theory only one activation foil per irradiation batch was necessary for accurate flux monitoring. All periphery target positions were symmetric about the center, so assuming a constant neutron flux and a 180° rotation about the target center at the irradiation midpoint, all targets should have been irradiated to equal dose. However, significant position dependent asymmetries in target irradiation were observed during both the third and fourth RadCCORE experiments. The most likely cause of the measured

asymmetries was misalignment of the target holder due to misalignment of the 0° telescope.

Several other factors also contributed to uneven irradiation of the targets, including changes in the deuteron current (and therefore neutron flux) during irradiation as well as the angular dependence of the neutron energy and flux. Since all the mouse targets were positioned off-axis, the neutron beam irradiated all the targets at an angle with a slightly different neutron energy, flux, and degree of target attenuation at each position along the mouse length. This effect can be minimized by irradiating the targets at greater distances from the gas cell, thereby reducing the irradiation angle (cf. third vs. fourth RadCCORE experiments). However, the target distance must still be small enough to ensure there is sufficient neutron flux to achieve reasonable irradiation times (~ few hours).

To decrease the necessary irradiation time for high dose target runs (i.e. 200-500 cGy irradiations), a liquid nitrogen cooled gas cell was developed. This gas cell held much more deuterium gas at comparable pressures as the standard air cooled cell, thereby increasing the effective target thickness and allowing for higher fluxes at increased distances. The increases gas thickness also led to a significant increase in the energy spread of the resultant neutron beam. Since the $^{27}Al(n,\alpha)^{24}Na$ reaction used to determine the neutron flux and dose to target is energy dependent, the accuracy of this measurement decreases significantly when the variation in neutron energy is large. Precise determination of the delivered dose is also complicated by the fact that the tissue kerma factors are also energy dependent, although to a lesser extent than the $^{27}Al(n,\alpha)^{24}Na$ reaction in the same energy regime. Minimizing the energy spread of neutrons produced

by the gas cell requires running at lower pressures which also reduces the neutron flux. However, lower gas cell pressures and greater target distances may be necessary in order to perform high precision irradiations and dose measurements using current techniques.

10.2 Possibilities for the Future

As previously noted, the current activation foil based approach to dose measurement has several significant drawbacks. The activation foils and mouse targets are exposed to a range of high energy neutrons as a consequence of the finite length of the gas cell and the targets being off-axis. The foils and mice are also exposed to low energy neutrons from room scatter and background which impart dose to the mice, but to which the aluminum activation foils are insensitive. Of course, even under the best of conditions, each monitor foil accurately relays the neutron fluence at only a single position (i.e. the head or tail of the mouse).

In the last several years, research into tissue equivalent gels (ex. MAGIC) and polyurethane based dosimeters (ex. PRESAGE®, Heuris Pharma LLC, Skillman, NJ) has grown exponentially. As opposed to activation foils (1-D) or radiochromic film (ex. 2-D Gafchromic® film) (2-D), the newest radiochromic gel and polyurethane dosimeters can be molded/cut into any desired shape and provide a 3-D view of the dose distribution throughout the material. The dose-response of these dosimeters to gamma radiation is well known and there have also been limited tests with high LET radiation[1]. Most research testing the response of these dosimeters to neutron radiation has focused on the thermal and epithermal energy regimes which are of the greatest interest in regard to

[1] Baldock et. al.

medical applications (ex. BNCT – Boron Neutron Capture Therapy)[2]. A great opportunity exists to use the facilities at TUNL to measure the response of these 3-D dosimeters to fields of fast neutrons. If the dose-response of the material(s) is sufficiently sensitive and can be calibrated against current techniques (i.e. foil activation), this research could prove invaluable for future small animal irradiation experiments at TUNL.

[2] Uusi-Simola et. al.

11. Ionization Chamber Measurement

11.1 Introduction

Neutron production via the $^{2}H(d,n)^{3}He$ reaction leads to the creation of secondary gamma radiation through several distinct processes. Elastic neutron scattering off beam-line and gas cell components, shielding materials within the target room, and the surrounding concrete walls leads to the production of excited nuclear states which then decay back to the ground state via emission of one or several gamma-rays. As these gamma-rays are prompt (~ few picoseconds), they are directly correlated with the neutron beam energy and flux. Gamma-rays are also produced through activation of the aforementioned materials, especially of the Havar® entrance foil and tantalum beam stop within the gas cell. These gamma-rays are produced through the decay of multiple isotopes (including ^{54}Mn, ^{56}Co, ^{57}Co, ^{58}Co, ^{85m}Kr, ^{109}Cd, etc.) each having different half-lives, creating a gamma background that builds up over time during the course of target irradiation. In order to perform high accuracy dosimetry of small animal targets at TUNL, detailed knowledge of the total gamma-ray contribution to target dose from both sources is required.

11.2 Ionization Chamber Descriptions and Theory

Two Far West Technology ionization chambers (Far West Technology, Inc., Goleta, CA) having different sensitivities to neutron and gamma radiation were used to determine the approximate percent contribution of the gamma component of the neutron beam to the total tissue dose at several incident neutron energies. The first ionization chamber (Model # IC-17) was made of tissue equivalent (TE) plastic and filled with methane-based tissue equivalent gas (64.4% CH_4, 32.5% CO_2, 3.1% N). The density and

percent by mass elemental composition of TE plastic and TE gas are listed in **Table 11.2.1**. The TE-TE chamber held 1 cm^3 of gas and had an inside diameter of 0.5 in and wall thickness of 0.2 in (569 mg/cm^3). The other chamber (Model #IC-17G) was made of graphite (C) and filled with carbon dioxide (CO_2) gas. The C-CO_2 chamber held 2 cm^3 of gas and had an inside diameter of 0.622 in and wall thickness of 0.119 in (543 mg/cm^3).

Table 11.2.1. Percent By Mass Elemental Composition of TE Plastic, TE Gas, and ICRU 46 Muscle.

Element	TE Plastic[1] (ρ = 1.127 g/cm^3)	TE Gas[1] (ρ = 1.064 x 10^{-3} g/cm^3)	ICRU 46 Muscle[2]
H	10.1327	10.1869	10.2
C	77.5501	45.6179	14.3
N	3.5057	3.5172	3.4
O	5.2316	40.6780	71.1
F	1.7422	-	-
Ca	1.8378	-	-

TE-TE chambers have approximately equal sensitivities to neutron and gamma radiation, while C-CO_2 chambers have relatively low neutron sensitivity. It is readily apparent from **Table 11.2.1** that both TE plastic and gas contain roughly equal hydrogen and nitrogen content to that contained in ICRU 46 Muscle, but radically different amounts of carbon and oxygen. However, this discrepancy does not strongly affect the tissue equivalency of the materials. Even though a large variety of neutron reactions (including elastic and inelastic scattering, (n,p), and (n,α)) occur in the constitute elements that make up biological tissues, only a few contribute significantly to the total kerma. The primary reactions of consequence depend on the incident neutron energy and the size of the tissue sample.

[1] National Institute of Standard and Technology (NIST)
[2] ICRU Report 46 (pg. 12)

At thermal energies, $^{1}H(n,\gamma)$ and $^{14}N(n,p)$ are the primary contributors to kerma.[3] When hydrogen captures an s-wave neutron to produce deuterium, a capture gamma-ray is emitted at 2.225 MeV (i.e. the neutron separation energy for ^{2}H). Naturally, these gamma-rays do not contribute to kerma until transferring energy to charged particles. For small tissue samples (dimensions << mean free path), most of these gamma-rays escape resulting in nearly all kerma being due to $^{14}N(n,p)$. For reference, the mean free path for 2.225 MeV gamma-rays in ICRU 46 Muscle is approximately 20.4 cm.

For fast neutrons, the total kerma in tissue is due almost exclusively to recoil protons from neutron elastic scattering off of hydrogen. Assuming this scattering is roughly isotropic, the average energy transferred to a given nuclei through neutron elastic scattering is approximated by: $\overline{E}_{tr} = E\frac{2M_a M_n}{(M_a+M_n)^2}$, where E is the neutron energy, M_a is the mass of the target nuclei, and M_n is the neutron mass. When the target nucleus is hydrogen, the average energy transferred is ½ the energy of the incident neutron. Hydrogenous materials are therefore excellent moderators of neutron radiation. By contrast, the average energy per collision transferred by elastic scattering is 0.142E for carbon, 0.124E for nitrogen, and 0.083E for oxygen[3].

As fast neutrons were utilized in the present experiment, the total kerma produced in the TE-TE ionization chamber was primarily due to the aforementioned ^{1}H(n,elastic) process. The kerma in the C-CO_2 chamber, by contrast, is produced mainly by carbon and oxygen heavy ions from neutron elastic scattering. Cross section plots for the significant kerma producing reactions for both chambers for fast neutrons are in **Appendix E**.

[3] Attix (Chapter 16)

11.3 Experiment Setup and Description

The first ionization chamber measurements in February of 2009 were conducted in the TUNL Time-of-Flight room using the same 6 cm gas cell as in the RadCCORE experiments. The TE-TE and C-CO_2 ionization chambers were placed back-to-back along the 0° beam axis. The C-CO_2 chamber was placed 10.2 cm from the center of the gas cell, while the TE-TE chamber was placed at a distance of 13 cm. Aluminum activation foils were placed in front of each ionization chamber to serve as monitors of the incident neutron flux. The front activation foil (in front of the C-CO_2 chamber) was 7.8 cm from the center of the gas cell, while the back foil (in front of the TE-TE chamber) was at a distance of 11.6 cm. To monitor the neutron flux live over the course of the experiment, a plastic scintillator paddle was placed at 0° behind the target setup 71.6 cm from the center of the gas cell. A liquid scintillation detector was also placed 11.5° off-axis at 514 cm (measured from the center of the gas cell to the detector face). A diagram of the setup can be seen in **Figure 11.3.1**.

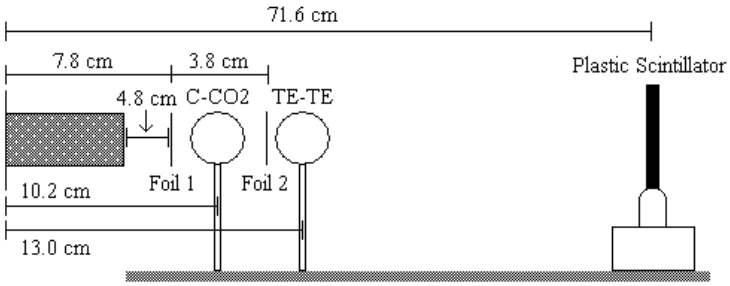

Figure 11.3.1. Ionization chamber setup.

For proper operation, the ionization chambers required a gas flow rate of approximately 5 cm^3/min. Precise monitors for such low flow rates were not available so

the gas flowing into each chamber was first bubbled though a solution of mineral oil. This technique allowed the flow rate to be accurately estimated by measuring the rate and size of the bubbles produced. Mineral oil was used in place of water in order to prevent moisture being added to the gas mixture. The gas pressure regulators on the TE and CO_2 gas bottles were found to be too course to achieve low flow rates so secondary needle values were added to achieve the necessary flow control. The final gas flow rates achieved were ~ 6.4 cm^3/min for the TE-TE chamber and 5.7 cm^3/min for the C-CO_2 chamber. Each ionization chamber was connected to an electrometer set to integrate mode, which measured the total charge (in coulombs) induced in the electrometer by incident radiation. The electrometer data was read and logged by a LabView® (National Instruments Corporation, Austin, TX) program specifically written for the measurements in this experiment.

Two series of irradiations were carried out at initial neutron energies of 8 and 10 MeV, respectively. Each irradiation series began with the gas cell at standard operating pressure (~ 7.8 atm). The target setup was then irradiated for several hours to allow sufficient activity to be induced in the monitor foils. The monitor foils were then removed. Several successive ionization chamber measurements were taken at approximately ¾, ½, and ¼ the initial gas cell pressure. The prompt gamma-ray flux was assumed to be proportional to the deuteron beam current. Therefore, lowering the gas cell pressure while keeping the beam current constant would lower the neutron yield and result in a greater percentage of the charge induced in the ionization chambers being due to gamma radiation. However, decreasing the deuterium pressure in the gas cell necessarily reduced the mass thickness of the gas which resulted in an increase in the

mean neutron energy as well as a decrease in the neutron energy spread. Details of the gas cell pressure, neutron energy and energy spread, irradiation time, and average beam current for both sets of irradiations are given in **Tables 11.3.1 and 11.3.2**.

Several background runs were also conducted with the ionization chambers before and after the in-beam measurements. Before irradiation, a measurement was made of the leakage current of both chambers in the absence of a radiation field. The current induced in the TE-TE chamber in the absence of a radiation field was found to be 9.847 x 10^{-15} A, while that for the C-CO_2 chamber was found to be 1.109 x 10^{-14} A. The measured values were marginally higher than the manufacturer specifications of less than 2 x 10^{-15} A. The charge induced in the ionization chamber by non-prompt gamma activity at the target position (caused by activation of the gas cell components) was also measured before and after the in-beam measurements. However, since the current induced from the non-prompt gamma-rays was on the order of the ionization chamber leakage currents (i.e. near zero signal-to-noise ratio), this data was not analyzed.

Table 11.3.1. Ionization Chamber 8 MeV Irradiation Run Data.

Neutron Energy (MeV)	Pressure (psi)	Irrad. Time (min)	Ave. I (μA)
8.02 + 0.590 / - 0.670	111.7	142.8	2.12
8.17 + 0.440 / - 0.480	84.0	37.1	2.19
8.32 + 0.290 / - 0.300	55.6	24.5	2.10
8.32 + 0.290 / - 0.300	55.6	26.9	2.12
8.47 +/- 0.140	27.4	21.3	2.12

Table 11.3.2. Ionization Chamber 10 MeV Irradiation Run Data.

Neutron Energy (MeV)	Pressure (psi)	Irrad. Time (min)	Ave. I (μA)
10.01 + 0.455 / - 0.485	113.3	108	2.46
10.12 + 0.340 / - 0.350	85.0	16.7	1.89
10.24 +/- 0.225	56.6	19	2.21
10.35 +/- 0.110	28.3	32.9	2.14
10.35 +/- 0.110	28.3	43.3	2.18

11.4 Analysis

The data obtained in the ionization chamber measurements was analyzed according to the procedure outlined in AAPM Report No. 7 and Attix's "Introduction to Radiological Physics"[3,4]. Calibration constants were provided by the ionization chamber manufacturer for the TE-TE and C-CO2 chambers for the gamma radiation produced by a ^{137}Cs source (3.21 x 10^9 R/C for the TE-TE chamber and 1.01 x 10^9 R/C for the C-CO2 chamber). These constants give the ratio of the exposure in *free space* produced at a given point from the calibration source to the charge produced in the ionization chamber with its center at the same position. The exposure rate at the calibration point was 65 R/hr. The charge collected in the ionization chamber from exposure to gamma radiation can be converted to tissue dose by the following factor: $A = \frac{1}{N_c \times f_{t,c} \times A_{w,c}}$, where A is the charge to dose constant for the calibration gamma radiation (i.e. the response per unit absorbed dose in tissue for gamma-rays – C/Gy), N_c is the gamma-ray calibration constant provided by the manufacturer for the ionization chamber (R/C), $f_{t,c}$ is the exposure to tissue dose conversion factor (Gy/R), and $A_{w,c}$ is a correction factor for attenuation and scatter in the ionization chamber walls compared to air. The factor $f_{t,c}$ is given by $f_{t,c} = 2.58 \times 10^{-4} \frac{C/kg}{R} \times 33.97 \frac{J}{C} \times \frac{(\mu_{en}/\rho)_{t,c}}{(\mu_{en}/\rho)_{air,c}}$,

where 33.97 J/C is the average energy to create an ion pair in dry air by secondary electrons created by the calibration photons (i.e. the electron W-value for air) and $\frac{(\mu_{en}/\rho)_{t,c}}{(\mu_{en}/\rho)_{air,c}}$ is the ratio of the mass energy absorption coefficients for tissue compared to

[4] AAPM Report No. 7

air at the calibration photon energy. As a precise value for $A_{w,c}$ for the chambers used was not available, it was estimated according to the following formula: $A_{w,c} = \frac{e^{-(\mu/\rho)_{w,c} \times m_{t,w}}}{e^{-(\mu/\rho)_{air,c} \times m_{t,air}}}$, where $(\mu/\rho)_{w,c}$ and $(\mu/\rho)_{air,c}$ are the mass attenuation coefficients (in cm^2/g) for the calibration gamma-rays in the ionization chamber wall material and air, respectively, $m_{t,w}$ is the mass thickness of the ionization chamber walls (0.569 g/cm^2 for the TE-TE chamber and 0.543 g/cm^2 for the C-CO2 chamber), and $m_{t,air}$ is the mass thickness of a wall of air equal in absolute thickness (cm) to the corresponding ionization chamber wall. The value of A as calculated above is technically only applicable to gamma radiation of the calibration energy (i.e. 662 keV gamma-rays produced from decay of ^{137}Cs). However, the response of the TE-TE and C-CO_2 ionization chambers to gamma radiation is constant over a wide energy range, hence the sensitivity relative to the calibration energy can be considered to be unity. Thus, the dose to the ionization chamber due to gamma radiation alone is given by: $D_{t,c} = \frac{Q_T}{A} = Q_T \times N_c \times f_{t,c} \times A_{w,c}$, where $D_{t,c}$ is the dose imparted to tissue by the gamma-ray field, Q_T is the measured charge collected in the ionization chamber, and the other quantities are as previously defined. The quantity $\frac{Q_T}{A}$ is the same as what is called R' in AAPM Report No. 7, although it is not explicitly defined in that publication.

In the mixed field scenario, the charge induced in the ionization chamber is not only due to secondary electrons created by incident gamma-rays, but also by a variety of other charged particles (i.e. p, α, heavy ion recoils) created by neutron interactions in the ionization chamber wall and gas. Generally, the W-value (average energy to create an ion

pair in the chamber gas by secondary charged particles) depends on both the charged particle type and energy. Likewise, the type, energy, and number of charged particles created by the neutron interactions depend on the incident neutron energy and nuclear cross sections for the reactions that create the charged particles in the chamber wall and gas. Thus, the ionization chamber will have a different dose response to neutrons than gamma-rays. The total charge collected in the ionization chamber from a mixed field measurement can be written as: $Q_{n,\gamma} = A \times D_\gamma + B \times D_n$, where $Q_{n,\gamma}$ is the total charge collected in the ionization chamber in the mixed field, *A* is the chamber dose response to gamma-rays, *B* is the chamber dose response to neutrons, and D_γ and D_n are the gamma-ray and neutron dose components, respectively. The constant, *B*, is generally not determined directly, but rather the ratio of *B/A*. With respect to the terminology of AAPM Report No. 7, *B/A* is equal to *k*.

The ratio *B/A* can be calculated explicitly for a tissue equivalent chamber (for which $k_T = (B/A)_T \sim 1$ – see **Section 11.2**). The dose response of the tissue equivalent chamber to neutrons relative to the gamma-rays used for calibration is given by:

$$k_T = \frac{\overline{W}_c}{\overline{W}_n} \times \frac{S_c}{S_n} \times \frac{K_c}{K_n},$$

where

$\overline{W}_c$ is the average energy to create an ion pair in the chamber gas by calibration photons (29.2 J/C for TE gas),

$\overline{W}_n$ is the average energy to create an ion pair in the chamber gas by secondary charged particles created by the neutron beam,

S_c is the ratio of mass collision stopping powers of the chamber wall to the filling gas averaged over the charged particle spectrum created by calibration gamma-rays,

S_n is the same ratio averaged over the charged particle spectrum created by incident neutrons,

$K_c = \frac{(\mu_{en}/\rho)_t}{(\mu_{en}/\rho)_w}$ is the ratio of the mass-energy absorption coefficients of tissue relative to A-150 plastic for the calibration photons, and

K_n is the neutron kerma factor ratio for muscle tissue relative to A-150 plastic.

Detailed calculations have been performed to determine the value of $\overline{W}_n$ for methane-based tissue equivalent gas over a wide range of neutron energies[5]. The values S_c and S_n have been experimentally measured and determined to be approximately equal to 1 and 1.01, respectively for TE-TE chambers[4]. Likewise, the values of K_c and K_n can be readily determined using the abundant tabulated data available from NIST[1], ICRU 46[2], and Attix[3].

The relative neutron sensitivity of a neutron insensitive ionization chamber (such as the C-CO[2] chamber), k_u, can generally not be calculated from theory but must be measured experimentally. Experimentally determined values of both k_T and k_u from Waterman et. al. were used[6]. Their measurements were made using the same model ionization chambers (IC-17 and IC-17G) as used in the present work. The k_T and k_u values used for the present measurements are given in **Table 11.4.1**. Exact values were available from the literature at 8 and 10 MeV. Values at other energies were determined through linear interpolation of the available tabulated data. The sensitivity of both chambers is approximately linear between 8 and 10.5 MeV. Therefore, this approach should introduce minimal additional error to the measurement results.

---

[5] Taylor et. al.
[6] Waterman et. al.

Table 11.4.1. TE-TE and C-CO_2 Relative Sensitivities by Neutron Energy.

Energy (MeV)	k_T (TE-TE Chamber)	k_U (C-CO_2 Chamber)
8.02	0.956	0.090
8.17	0.956	0.093
8.32	0.955	0.096
8.47	0.955	0.098
10.01	0.951	0.135
10.12	0.950	0.139
10.24	0.950	0.143
10.35	0.949	0.147

Putting all the known information together, $\frac{Q_{T,TE}}{A_{TE}} = D_\gamma + k_T \times D_n$, where $Q_{T,TE}$ is the total charge measured for the TE-TE chamber in the mixed radiation field, and $\frac{Q_{T,CO_2}}{A_{CO_2}} = D_\gamma + k_U \times D_n$, where Q_{T,CO_2} is the total charge measured for the C-CO_2 chamber for an identical irradiation in the mixed field at the same position as the TE-TE chamber. Setting $\frac{Q_{T,TE}}{A_{TE}} = R'_{TE}$ and $\frac{Q_{T,CO_2}}{A_{CO_2}} = R'_{CO_2}$ and solving for the separate neutron and gamma dose components, D_n and D_γ, gives:

$$D_n = \frac{R'_{TE} - R'_{CO_2}}{k_T - k_U} \text{ and}$$

$$D_\gamma = \frac{k_T \times R'_{CO_2} - k_U \times R'_{TE}}{k_T - k_U}.$$

The total dose to tissue from the mixed field at the ionization chamber position is given by: $D_{T,n\gamma} = D_n + D_\gamma$. The fraction of total dose due to gamma radiation alone (i.e. the gamma dose fraction), f_γ, is thus given by $f_\gamma = \frac{D_\gamma}{D_n + D_\gamma}$.

Given the difficulty in achieving an identical mixed field irradiation of each ionization chamber individually at a single target position, the decision was made to irradiate both ionization chambers simultaneously. As detailed in **Section 11.3**, the TE-TE and C-CO2 chambers were placed back to back along the 0° beam axis. Thus, for the percent gamma contribution to dose to be determined, corrections had to be made for the different ionization chamber distances from the gas cell and the attenuating effect of the front C-CO_2 ionization chamber. The C-CO_2 ionization chamber data was adjusted down (i.e. multiplied by a distance correction factor) to account for the greater distance from the gas cell of the TE-TE chamber, while the TE-TE chamber data was adjusted up (i.e. divided by an attenuation correction factor) to compensate for the reduced flux caused by the attenuation of the C-CO_2 chamber. A direct comparison of the readings between the two chambers was then possible.

The distance correction was made by approximating the gas cell as a cylindrical source with a uniform activity distribution. The general formula for the flux fall-off from a space source is given by: $G(\vec{r}) = \dfrac{\int_V \frac{\rho(\vec{r}')dV'}{|\vec{r} - \vec{r}'|^2}}{\int_V \rho(\vec{r}')dV'}$, where $\rho(\vec{r}')$ is the density function for the radiative material within the source, and $\vec{r}$ and $\vec{r}'$ are vectors defining points of measurement outside the source and radiative points inside the source, respectively[7]. For, a uniform source, $\rho(\vec{r}')$ = ρ (i.e. ρ is a constant). In this case, the preceding equation reduces to $G(\vec{r}) = \dfrac{1}{V_s}\int_V \frac{dV'}{|\vec{r} - \vec{r}'|^2}$, where V_s is the volume of the source. For the case of a

[7] Baltas (Chapter 8).

uniformly irradiating cylinder, the flux fall-off at a point along the longitudinal (z) axis is given by: $G(\vec{r}) = \frac{1}{\pi \times R^2 \times L} \int_{-L/2}^{L/2} \int_0^{2\pi} \int_0^R \frac{\rho' \mathrm{d}\rho' \mathrm{d}\phi' \mathrm{d}z'}{\rho'^2 + (z - z')^2}$,

where R is the radius of the cylinder (i.e. the gas cell radius – 0.4 cm), L is the length of the cylinder (i.e. the length of the gas cell – 6 cm), and z is the distance from the center of the cylinder along the longitudinal axis (i.e. distance from the gas cell). For the ionization chamber distances listed in **Figure 11.3.1**, the distance correction factor for the C-CO_2 chamber was found to be 0.594 (i.e. the neutron flux at the TE-TE chamber position was 0.594 times the flux at the C-CO_2 chamber position). This value was found to be close to that predicted assuming the standard point source model (i.e. $1/r^2$ flux fall-off).

The correction for the attenuation of the neutron beam by the C-CO_2 chamber was estimated by calculating the attenuation of a uniform rectangular slab with length and width equal to the diameter of the ionization chamber and volume equal to the volume of the ionization chamber's graphite shell (i.e. equal amount of material). Given the dimensions of the C-CO_2 ion chamber provided in **Section 11.2**, the corresponding rectangular slab of equal volume was found to have a thickness of 0.711 cm, which corresponded to an atomic thickness of 6.417 x 10^{22} atoms/cm^2. The attenuation correction was then estimated to be $e^{-\sigma(E)*a_t}$, where $\sigma(E)$ is equal to the ^{12}C(n,total) cross section (in cm^2) at the relevant neutron energies given in **Tables 11.3.1** and **11.3.2**, and a_t is the atomic thickness (atoms/cm^2) of the graphite shell. The attenuating effect of the chamber gas can be considered negligible. The ^{12}C(n,total) cross sections and corresponding attenuation corrections at each neutron energy at given in **Table 11.4.2**.

Error estimates for the individual quantities that go into the gamma dose fraction calculation can be found in **Appendix F**.

Table 11.4.2. ^{12}C(n,total) Cross Sections and Attenuation Corrections by Neutron Energy.

Neutron Energy (MeV)	^{12}C(n,tot) σ (x 10^{-24} cm^2)[8]	Atten. Correction
8.02	1.852	0.888
8.17	1.652	0.899
8.32	1.234	0.924
8.47	1.105	0.932
10.01	1.168	0.928
10.12	1.127	0.930
10.24	1.113	0.931
10.35	1.130	0.930

The total tissue dose to target can also be calculated with a single TE-TE chamber. In general, the total dose to tissue measured by the ionization chamber is given by: $D_{t,T} = D_n + D_\gamma = \frac{Q_n}{M_g} \times \overline{W}_n \times S_n \times K_n + \frac{Q_\gamma}{M_g} \times \overline{W}_\gamma \times S_\gamma \times K_\gamma$,

where M_g is the mass of the chamber gas (in kg), Q_n is the portion of the ionization chamber charge due to neutron radiation, Q_γ is the portion of the charge due to gamma radiation, $\overline{W}_n$, S_n, and K_n are defined as previously, and $\overline{W}_\gamma$, S_γ, and K_γ are defined similarly to $\overline{W}_c$, S_c, and K_c, only for the actual incident gamma-rays opposed to the calibration gammas. Substituting in $Q_n = Q_T - Q_\gamma$, then

$$D_{t,T} = \frac{Q_T}{M_g} \times \overline{W}_n \times S_n \times K_n \times \left(1 - \left(1 - \frac{\overline{W}_\gamma \times S_\gamma \times K_\gamma}{\overline{W}_n \times S_n \times K_n}\right) \times \frac{Q_\gamma}{Q_T}\right).$$

[8] NNDC.

Defining a new quantity $h_T = \frac{\overline{W}_c \times S_c \times K_c}{\overline{W}_\gamma \times S_\gamma \times K_\gamma}$, where h_T is the sensitivity of the TE-TE chamber to the incident gamma-rays relative to the calibration gamma-rays, then

$$D_{t,T} = \frac{Q_T}{M_g} \times \overline{W}_n \times S_n \times K_n \times \left(1 - \left(1 - \frac{k_T}{h_T}\right) \times \frac{Q_\gamma}{Q_T}\right).$$

The quantity h_T is generally equal to 1 (the sensitivity of the ionization chamber to gamma-rays is constant over a wide energy range as previously noted) and when the charge ratio $\frac{Q_\gamma}{Q_T}$ is small (< ~ 0.2, i.e. 20% of dose due to gamma-rays), the total quantity in parenthesis is ~ 1. Also, in terms of previously defined quantities, $M_g = A \times \overline{W}_c \times S_c \times K_c$. Making this final substitution, the relatively lengthy equation above reduces simply to $D_{t,T} = \frac{Q_T}{A \times k_T}$. This equation is identical to the prior listed equation $\frac{Q_{T,TE}}{A_{TE}} = D_\gamma + k_T \times D_n$ with D_γ set equal to zero.

When the equivalent dose, $H_t = Q \times D_t$, for a biological target in a mixed source beam is required, a dual chamber measurement is necessary if the gamma dose component is suspected to be non-negligible. Otherwise, the effective dose will be overestimated. When the percent of the total dose due to gamma-rays is known, a correction factor can be made to the dose measured using the single TE-TE chamber to avoid overestimation. Since the dose fraction is approximately equal to the charge ratio $\frac{Q_x}{Q_T}$ (where x = γ or n)[4], then using a single TE-TE chamber: $D_n = \frac{Q_T}{A \times k_T} \times (1 - DF)$ and

$D_\gamma = \frac{Q_T}{A} \times DF$, where DF is the experimentally measured gamma-ray dose fraction determined with the two chamber technique.

11.5 Results

The results of the third RadCCORE experiment are given in **Tables 11.5.1-11.5.5**. In **Tables 11.5.1** and **11.5.2**, the columns labeled "TE-TE Charge" and "C-CO_2 Charge" give the total background subtracted charge collected in the ionization chambers during the given irradiation. The "R' (TE-TE)" and "R'(C-CO_2)" columns give the R' values for the TE-TE and C-CO_2 ionization chambers calculated according to the relevant equation given on page 70 (i.e. Q/A). The "R' Corr." column in **Table 11.5.1** gives the values of R' corrected for neutron attenuation by the C-CO_2 ionization chamber according to the procedure outlined on page 72. The "R' Corr." column in **Table 11.5.2** gives the values of R' corrected for the C-CO_2 ionization chamber corrected for distance according to the procedure outlined on pages 71 and 72. The gamma dose fraction (i.e. %γ) given in **Table 11.5.3** was determined according to the procedure outlined on page 70. In **Table 11.5.4**, the neutron flux was determined in the same manner as in the RadCCORE series of experiments. The reported dose values were determined using the relevant neutron kerma factors for muscle tissue at 8 MeV (5.27 x 10^{-9} cGy cm^2/n) and 10 MeV (5.72 x 10^{-9} cGy cm^2/n), respectively. For **Table 11.5.5**, in order to compare the dose measured by the back activation foil (in front of the TE-TE chamber) with the dose measured by the TE-TE chamber, distance and surface area corrections were made to the foil results for Foil 2 from **Table 11.5.4**. The distance correction was calculated according to the procedure outlined on pages 71 and 72 in order to determine the dose the foil would have

received if it was positioned at the ion chamber center. This distance correction was equal to 0.785. A surface area correction was also necessary since the activation foil diameter was slightly larger than the foil diameter. The surface area correction was calculated as the square of the ratio of the ion chamber diameter to the foil diameter and was found to be 0.836. The total correction factor to the foil data was therefore 0.656. The foil values were compared to the dose measured from the TE-TE ionization chamber, which was taken to be the uncorrected R' value at the relevant neutron energy (i.e. 8 or 10 MeV) (see **Table 11.5.1**) multiplied by 1 minus the gamma dose fraction at that energy.

Table 11.5.1. Collected charge, R', and R' w/ neutron attenuation correction for the TE-TE chamber as a function of neutron energy and gas cell pressure.

E_n (MeV)	P (psi)	TE-TE Charge (C)	R'(TE-TE) (mGy)	R' Corr. (mGy)
8.02	111.7	1.002×10^{-7}	2959	3333
8.17	84.0	2.108×10^{-8}	623	692
8.32	55.6	9.237×10^{-9}	273	295
8.32	55.6	1.026×10^{-8}	303	328
8.47	27.4	4.450×10^{-9}	131	141
10.01	113.3	1.379×10^{-7}	4073	4390
10.12	85.0	1.337×10^{-8}	395	424
10.24	56.6	1.204×10^{-8}	356	382
10.35	28.3	1.145×10^{-8}	338	364
10.35	28.3	8.072×10^{-9}	238	256

Table 11.5.2. Collected charge, R', and R' w/ distance correction for the C-CO_2 Chamber as a function of neutron energy and gas cell pressure.

E_n (MeV)	P (psi)	C-CO_2 Charge (C)	R'(C-CO_2) (mGy)	R' Corr. (mGy)
8.02	111.7	7.003×10^{-8}	655	389
8.17	84.0	1.454×10^{-8}	136	81
8.32	55.6	6.515×10^{-9}	61	36
8.32	55.6	7.226×10^{-9}	68	40
8.47	27.4	3.461×10^{-9}	32	19
10.01	113.3	1.245×10^{-7}	1164	692
10.12	85.0	1.218×10^{-8}	114	68
10.24	56.6	1.109×10^{-8}	104	62
10.35	28.3	1.097×10^{-8}	103	61
10.35	28.3	7.568×10^{-9}	71	42

Table 11.5.3. Gamma dose fraction as a function of neutron energy and gas cell pressure for experimentally determined values of k_T and k_u and for k_T = 1.

E_n (MeV)	P (psi)	% γ	Upper Bound	% γ (k_T=1)	Upper Bound
8.02	111.7	2.4% ± 1.6	4.0%	2.9% ± 1.3	4.2%
8.17	84.0	2.0% ± 1.7	3.7%	2.6% ± 1.3	3.9%
8.32	55.6	2.4% ± 1.7	4.1%	3.0% ± 1.4	4.4%
8.32	55.6	2.4% ± 1.7	4.1%	2.9% ± 1.4	4.3%
8.47	27.4	3.5% ± 1.8	5.3%	4.2% ± 1.4	5.6%
10.01	113.3	1.7% ± 2.5	4.2%	2.6% ± 2.0	4.6%
10.12	85.0	1.5% ± 2.6	4.1%	2.4% ± 2.1	4.4%
10.24	56.6	1.2% ± 2.7	3.9%	2.1% ± 2.1	4.3%
10.35	28.3	1.5% ± 2.8	4.3%	2.5% ± 2.2	4.6%
10.35	28.3	1.1% ± 2.8*	3.9%	2.0% ± 2.2*	4.2%

*Neutron beam on with 5 cm lead placed in front of the gas cell.

Table 11.5.4. Neutron fluences and corresponding derived doses (using neutron kerma factors for muscle tissue) at Foil 1 (in front of C-CO_2) and Foil 2 (in front of TE-TE) positions.

E_n (MeV)	Foil 1 (n/cm^2/s)	Dose (cGy)	Foil 2 (n/cm^2/s)	Dose (cGy)
8.02	1.918 x 10^{11} ± 3.3%	1011 ± 33	8.880 x 10^{10} ± 3.3%	468 ± 16
10.01	1.554 x 10^{11} ± 3.3%	889 ± 29	7.372 x 10^{10} ± 3.4%	422 ± 14

Table 11.5.5. Foil 2 (in front of TE-TE) neutron dose corrected for distance and surface area vs. dose determined from the TE-TE Chamber.

E_n (MeV)	Foil 2 Dose Corrected (cGy)*	TE-TE Chamber Dose (cGy)
8.02	307 ± 24	302 ± 12
10.01	276 ± 22	421 ± 16

*Includes additional uncertainty from correction factors. See **Appendix F**.

11.6 Discussion and Summary

Using a dual ionization chamber technique, the gamma dose fraction for the monoenergetic neutron source at TUNL was successfully measured at several incident neutron energies. The currents induced in the TE-TE and C-CO_2 ionization chambers from charged particles produced by beam correlated neutron and gamma-ray interactions were several orders of magnitude higher than their respective leakage currents, even at low deuterium pressures. Using experimentally measured values of k_T and k_u for the TE-

TE and C-CO_2 chamber, respectively, the gamma dose fraction was found to be approximately 2.4% at 8 MeV and 1.7% at 10 MeV with ~ 7.8 atm of deuterium in the gas cell. The gamma dose fraction becomes 2.9% at 8 MeV and 2.6% at 10 MeV if the common assumption is made that, on average, k_T ~ 1 over the neutron energy spectrum from several hundred keV to 20 MeV. An increase in the gamma dose fraction was observed at 8 MeV as the gas cell pressure was lowered (as was expected), but the increase was relatively minor. At 10 MeV neutron energy, no significant increase in the gamma dose fraction with decreasing gas cell pressure was observed down to a deuterium pressure of ~ 2 atm.

Minor changes in the gamma dose fraction were difficult to observe due to the high degree of uncertainty in the small gamma dose component. Also, at higher neutron energies, the relative neutron sensitivity of the C-CO_2 chamber increases significantly, while the neutron sensitivity of the TE-TE chamber remains relatively constant. Thus, at higher energies, there is decreased discrimination between the gamma and neutron dose components (i.e. chamber readings become more similar in the mixed field) which increases the uncertainty in the gamma dose fraction.

Based on the previous measurements and uncertainties, the upper bound of the gamma dose fraction was determined to be 4.2% at 8 MeV and 4.6% at 10 MeV for the standard 7.8 atm gas cell pressure. The upper bound of the gamma dose fraction increased to 5.6% for 8 MeV neutrons when the gas cell pressure was 2 atm. These measured values of the gamma dose fraction are in agreement with the expected value of < 10%. Given the large difference in quality factors between gamma-rays (= 1) and fast

neutrons (~ 10), the gamma component of the beam therefore contributes negligibly to the equivalent dose imparted to biological tissue.

Since aluminum activation foils were used as flux monitors for the first runs (full gas cell pressure) at 8 and 10 MeV incident neutron energies, a comparison was made between the neutron dose calculated based on the foil measurements and the dose determined from the TE-TE ionization chamber. The foil measurements were analyzed in the same manner and using the same detector setup as in the RadCCORE experiments. The measured neutron fluences were converted to dose to muscle tissue using the relevant neutron kerma factors. Since the activation foil in front of the TE-TE chamber was slightly closer to the gas cell and of marginally greater diameter than the TE-TE chamber, corrections were made for these effects. In the final comparison, the neutron dose determined from the activation foil technique was in excellent agreement with the value determined from the TE-TE ionization chamber measurement at 8 MeV. However, at 10 MeV, the TE-TE ionization chamber measured a significantly higher dose than that determined based on the activation foil measurement. The large discrepancy cannot be explained at present. One possibility for the increased dose measured by the TE-TE chamber at 10 MeV is the influence of lower energy neutrons from deuteron breakup (i.e. $^{2}H(d,np)^{2}H$). However, the magnitude of the observed discrepancy is significantly larger than the expected contribution of these breakup neutrons to target dose based on prior measurements at TUNL.[9] An additional measurement should be performed at a future date to verify the 10 MeV results.

[9] Swartz.

11.7 Future Improvements for Ionization Chamber Measurements at TUNL

Several changes could be made to the experimental setup to improve the accuracy of future gamma dose fraction measurements. Ideally, the two ionization chambers should be given identical irradiations in the same target position. As this condition is difficult to achieve with an accelerator produced neutron source, an alternative solution is to position the ion chambers side by side at a fixed distance from the gas cell. This setup configuration would eliminate the need for distance and attenuation corrections for the dual chamber measurements. However, in such a setup, the ionization chambers would no longer be at 0° and the neutron flux and energy have an angular dependence, as has been previously established. Greater target distances will minimize the angle an off-axis target makes with the gas cell (and hence the drop-off in the $^{2}H(d,n)^{3}He$ differential cross section and neutron energy) at the expense of neutron flux. To minimize the differential cross section dependent flux drop-off (no more than 10% decrease vs. 0° value), the angle the target makes with the gas cell must be less than 6° (for 6.823 MeV incident deuterons producing 10 MeV neutrons at the center of the gas cell). At this angle, the corresponding drop-off in neutron energy is only 50 keV (0.5%). Given the diameter of both ionization chambers are ~ 1 in, the chambers must be positioned at a minimum 0° distance of 12 cm from the gas cell to achieve an angle of 6° or less between the center of the gas cell and the ionization chambers. During the February experiment, the TE-TE chamber was positioned 13 cm from the gas cell so it is known the neutron flux is sufficient at this distance to produce adequate current in the chamber using the standard 6 cm gas cell.

12. Concluding Remarks

The 2009 RadCCORE experiments and 2011 ionization chamber measurements at TUNL achieved all stated objectives. The methodology was developed to perform high accuracy neutron dosimetry of small animal targets using both a foil activation technique and live-time flux monitoring using liquid and plastic scintillation detectors. A dual ionization chamber technique was also successfully utilized to measure the gamma dose fraction at several distinct neutron energies for neutron beams produced via the $^{2}H(d,n)^{3}He$ reaction at TUNL. With the experience gained and results achieved from the recent gamma dose fraction measurements, real time dose monitoring of future small animal irradiation experiments using a single TE-TE chamber is now possible, providing a potentially more accurate tool for future neutron dosimetry work at TUNL.

Appendix A - Foil Measurement Sources of Error

The following is a list of all uncertainties in the neutron flux measurements for measured or calculated quantities whose uncertainty is 0.01% or greater.

Table A.1. Foil Measurement Sources of Error.

Quantity	Uncertainty
Activation Product Half-Life	0.01%
Photopeak Area	0.5 – 2%
Detector Efficiency	3.2 / 4.7%
Irradiation Time Factor	0.6 – 1.4%
Decay Time Factor	< 0.1%
Measurement Time Factor	0.01%
Reaction Cross Section (Abs)*	~ 2 – 3% (Est.)
Cross Section Energy Variance**	2 – 4%
# Nuclei in Foil	0.1%
Measured Flux (Abs. Measurement)	3.3 – 5.2%
Measured Flux (Rel. Measurement)	~ 1%
Muscle Tissue Kerma Factors	~ 5%

*Note: The error in the reaction cross sections were not taken into account in the final error measurements since this error was estimated.

**Note: Only applicable to mouse measurements. The uncertainty in the calculated neutron flux incident on each foil, resulting from variance in the incident neutron energy (and thus the Al(n,α) cross section) at different foil positions due to rotation, was taken to be half of the total percent change in the cross section over the relevant energy range.

Appendix B – Detector Efficiency Curves

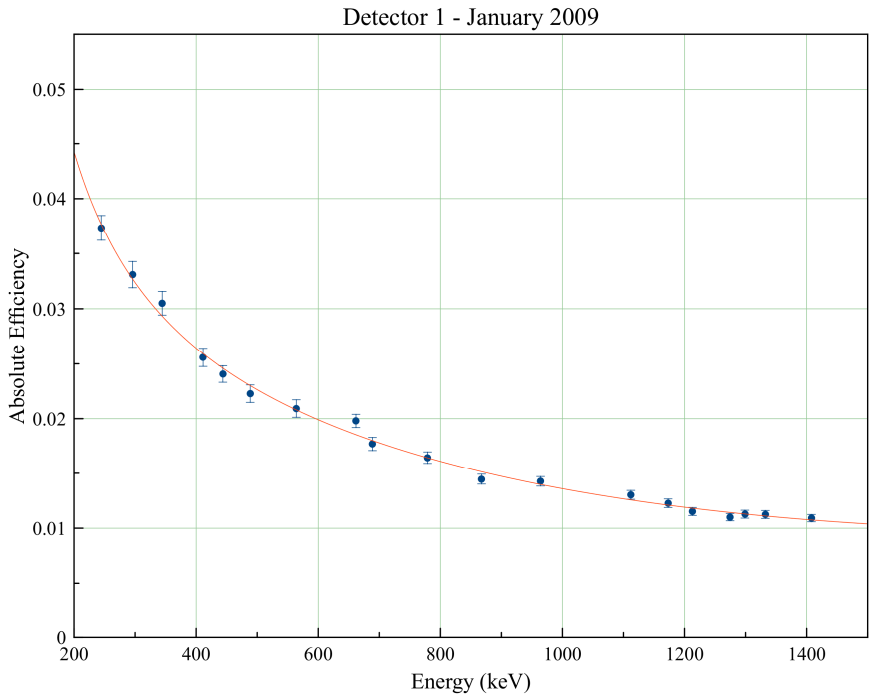

Figure B.1. Detector 1 Efficiency Curve – January 2009.

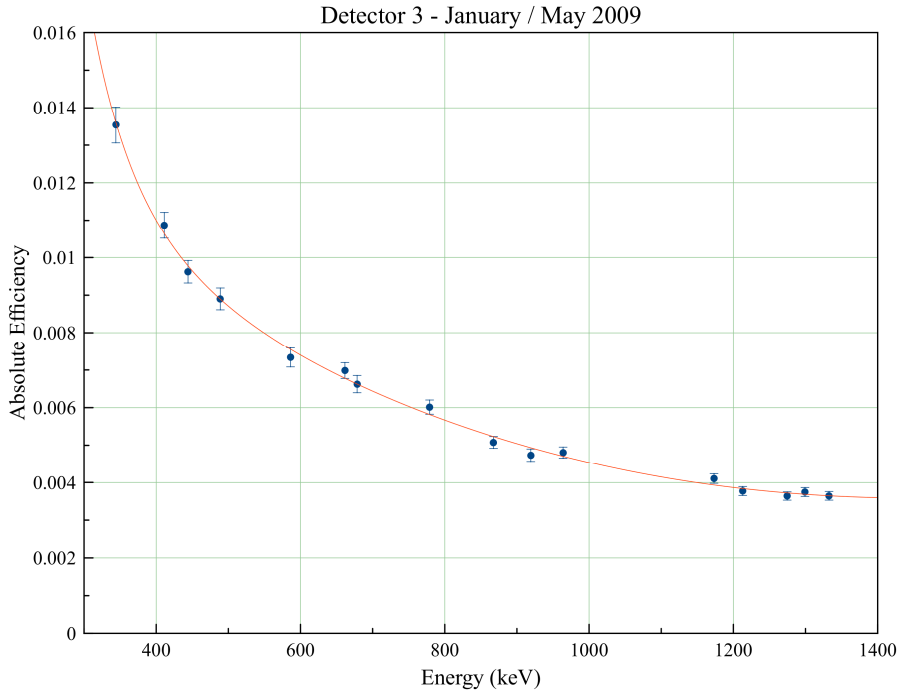

Figure B.2. Detector 3 Efficiency Curve – January / May 2009.

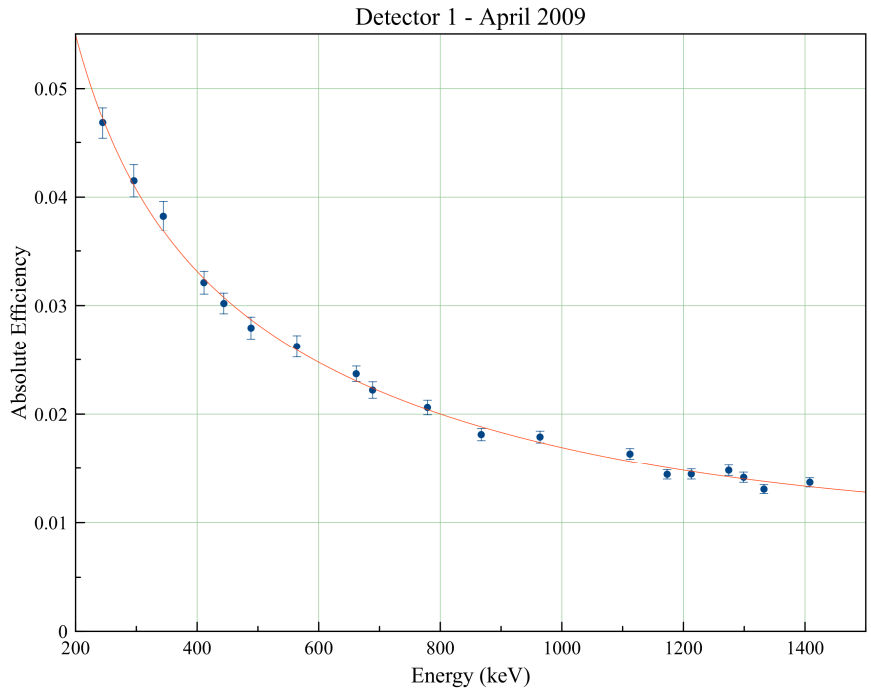

Figure B.3. Detector 1 Efficiency Curve – April 2009.

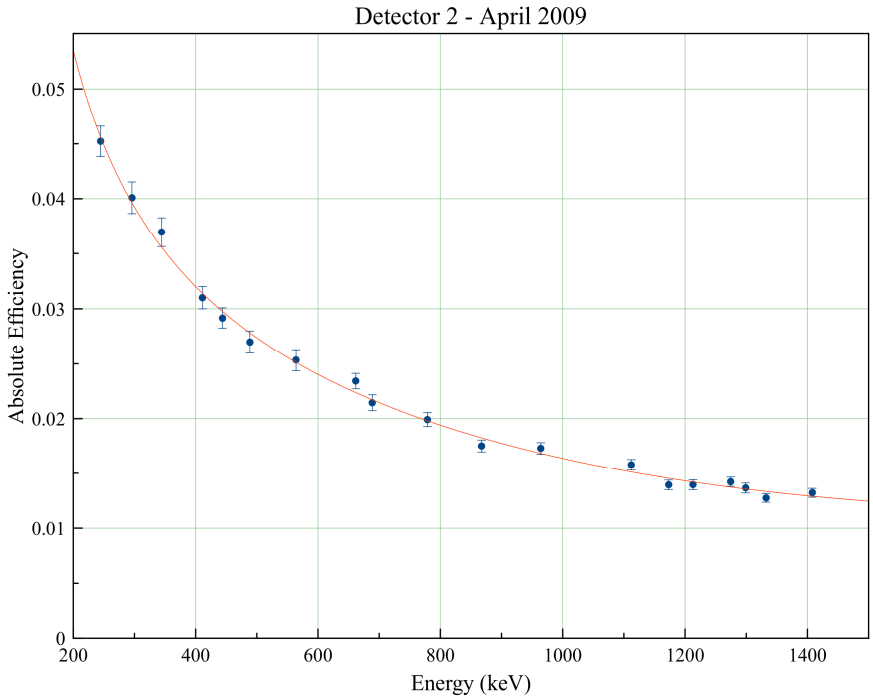

Figure B.4. Detector 2 Efficiency Curve – April 2009.

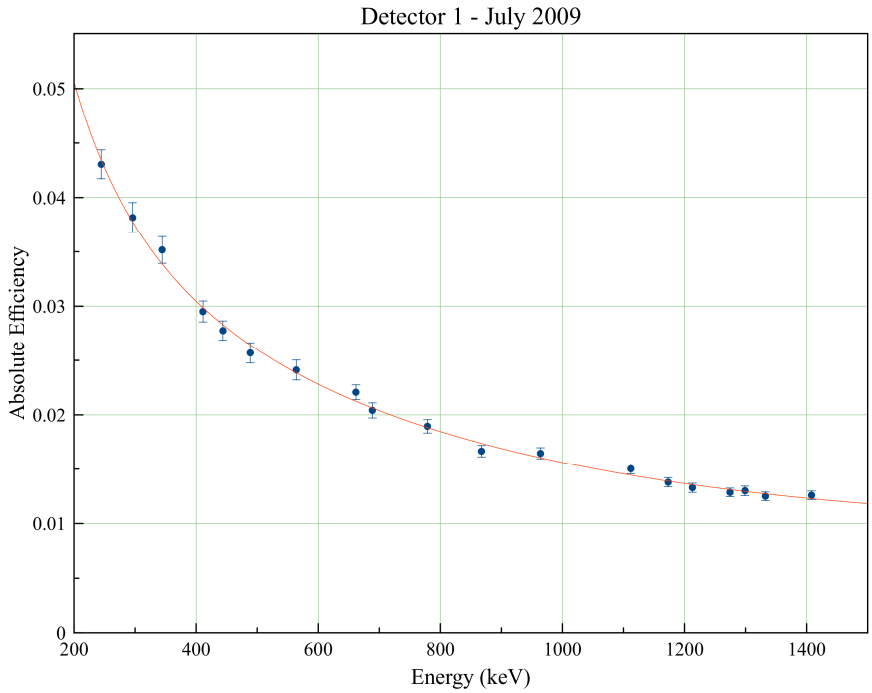

Figure B.5. Detector 1 Efficiency Curve – July 2009.

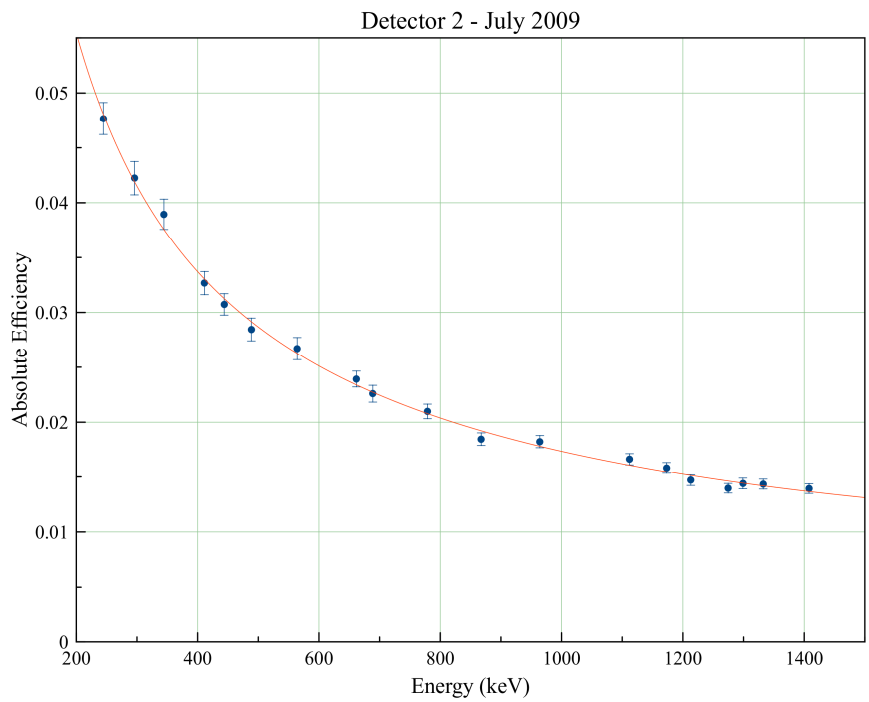

Figure B.6. Detector 2 Efficiency Curve – July 2009.

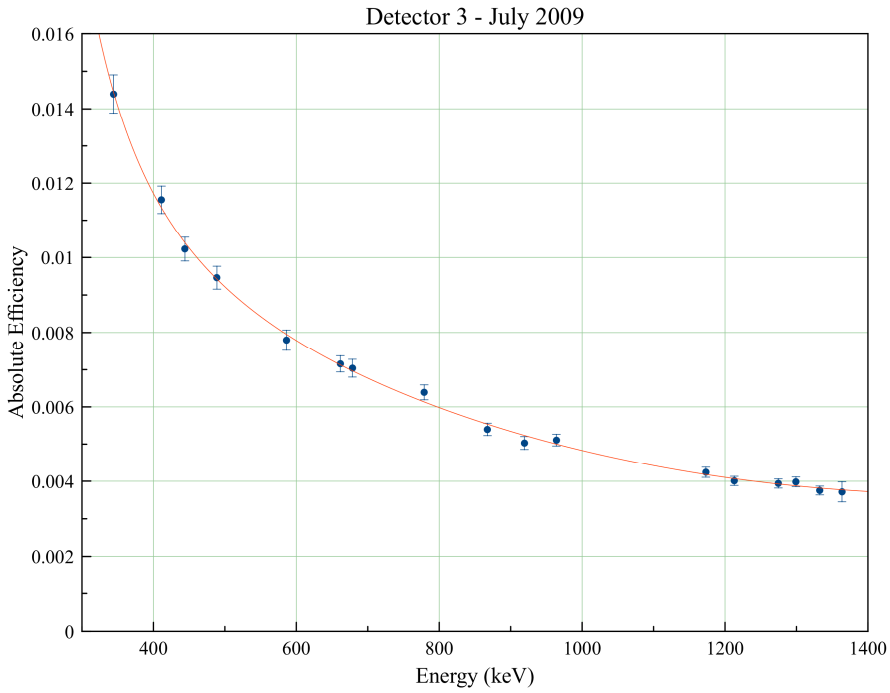

Figure B.7. Detector 3 Efficiency Curve – July 2009.

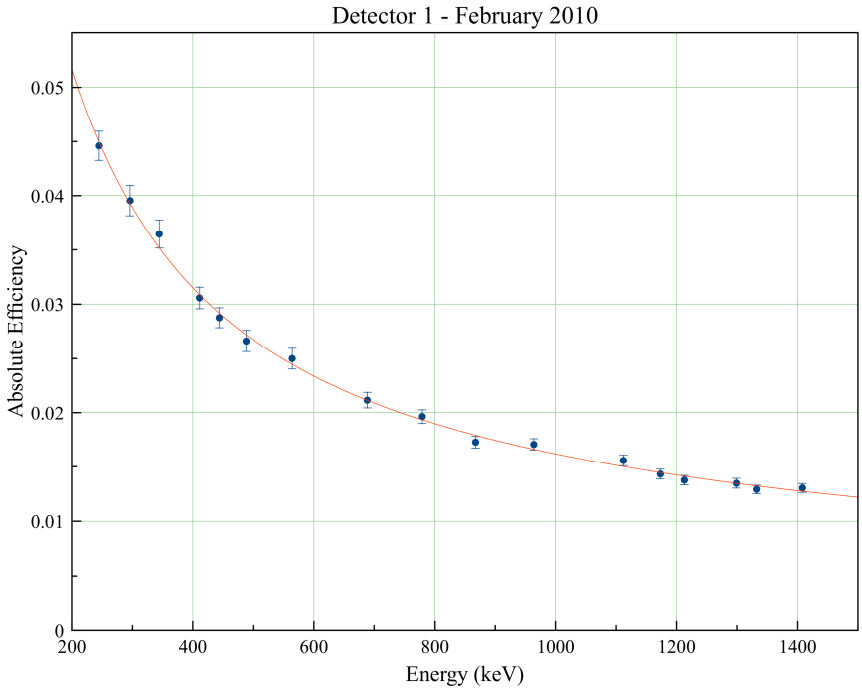

Figure B.8. Detector 1 Efficiency Curve – January 2010.

Appendix C - Dose Estimation Using an Off-Axis Liquid Scintillation Detector

A liquid scintillation detector placed at 60° with respect to the 0° axis was used to monitor the neutron flux in real time during the second and third RadCCORE experiments. The neutron fluence (and dose) at the target position was calculated utilizing kinematics and differential cross section data for the $^{2}H(d,n)^{3}He$ reaction, the neutron monitor and target distances (from the center of the gas cell) and cross-sectional areas, the neutron monitor efficiency, and the off-axis neutron flux reduction information obtained from the second RadCCORE experiment.

The number of neutrons incident upon the target position was calculated according to the following equation:

$$f_d(\theta_m) = f_r \times \frac{\sigma(0°)}{\sigma(60°)} \times \left(\frac{r_m}{r_d}\right)^2 \times \left(\frac{l_d}{l_m}\right)^2 \times \frac{1}{\varepsilon(E_n(60°))} \times f_m(60°),$$

where

f_r is the ratio of the fluence measured at the off-axis position of the target holder relative to 0° (~ 0.5),

$\sigma(0°)$ is the $^{2}H(d,n)^{3}He$ differential cross section at 0° (86.5 mb),

$\sigma(60°)$ is the differential cross section at 60° (8.09 mb),

r_m is the radius of the foil / mouse targets (1.25 cm),

r_d is the radius of the neutron detector (2.54 cm),

l_d is the distance of the neutron detector from the center of the gas cell (333.4 cm),

l_m is distance of the target from the center of the gas cell (calculated using the distance to the front face of the target holder - 11.5 cm),

$E_n(60°)$ is energy of the neutrons produced at 60° (6.5 MeV when $E_n(0°)$ = 10 MeV),

$\varepsilon(E_n(60°))$ is the efficiency of the detector for 6.5 MeV neutrons (0.20), and

$f_m(60°)$ is the number of neutrons measured by the 60° monitor during the irradiation time.

The dose to target is then given by the neutron fluence multiplied by the appropriate neutron kerma factor for muscle tissue (K = 5.647 x 10^{-9} cGy cm^2/n), i.e.,

$$D = \phi \times K = \frac{f_a(\theta_m)}{\pi \times r_m^{\ 2}} \times K \ .$$

The number of neutrons per cGy is given by:

$$\frac{Neutrons}{cGy} = \frac{f_m(60°) \times \pi \times r_m^{\ 2}}{f_a(\theta_m) \times K} \ .$$

Based on this approximation, a 1 cGy dose at the target position was found to correspond to 1.60 x 10^7 neutron counts in the 60° monitor.

Appendix D - Dose Estimation Using a Plastic Scintillator Paddle at 0°

A plastic scintillator paddle placed along the 0° beam axis was used for real-time flux monitoring during the fourth RadCCORE experiment. This paddle was the same one used in the first RadCCORE experiment. A single aluminum activation foil was placed in the center position of the target holder (0°) 20 cm from the center of the gas cell. The scintillator paddle was also placed at 0° behind the target holder 54.8 cm from the center of the gas cell. The target setup was then irradiated for 1 hour and 10 minutes at an average beam current of 1.56 μA. The average gas cell pressure over the course of the run was 96.3 psi (6.5 atm) at 77 K corresponding to 366.3 psi (24.9 atm) at room temperature (293 K). At this pressure, 7.125 MeV deuterons were produced at the center of the gas cell, leading to the production of 10.29 MeV neutrons at 0°. Since an activation foil of the same diameter as the mouse targets was used as an absolute flux monitor, and the foil and scintillator paddle were both placed along the 0° beam axis, the calculations for the number of neutrons and dose at the target position are more straightforward than those using the 60° monitor.

The number of neutrons incident upon the target position was calculated using the following equation:

$$f_d(\theta_m) = f_r \times \frac{n_f}{n_p} \times \left(\frac{d_1}{d_0}\right)^2 \times f_m(0°) ,$$

where

f_r is the ratio of the fluence measured at the off-axis position of the target holder relative to 0°,

n_f is the number of neutrons measured by the activation foil in the calibration run,

n_p is the number of neutrons measured by the scintillator paddle during the calibration run,

d_0 is the distance of the scintillator paddle from the center of the gas cell during the calibration run (54.8 cm),

d_1 is distance of the paddle from the center of the gas cell during the mouse irradiations (48.6 cm), and

$f_m(0°)$ is the number of neutrons measured by the 0° paddle during the irradiation time.

For the fourth RadCCORE experiment, the number of incident neutrons and dose to target were calculated to the center of the target holder as opposed to the front face as in the third RadCCORE experiment. No additional correction factor was necessary to compensate for a change in target distance since the activation foil during the calibration run was placed at the same distance as the center of the target holder during the mouse irradiations.

As in the 60° monitor case, the dose to target is given by:

$D = \phi \times K = \frac{f_d(\theta_m)}{\pi \times r_m^2} \times K$, where r_m is the mouse radius and K is the neutron kerma factor.

The number of neutrons per cGy is then:

$$\frac{Neutrons}{cGy} = \frac{f_m(0°) \times \pi \times r_m^2}{f_d(\theta_m) \times K}.$$

Based on this approximation, a 1 cGy dose at the target position was found to correspond to 8.46 x 10^6 neutron counts in the 0° scintillator paddle.

Appendix E – Principal Kerma Producing Reactions in Tissue

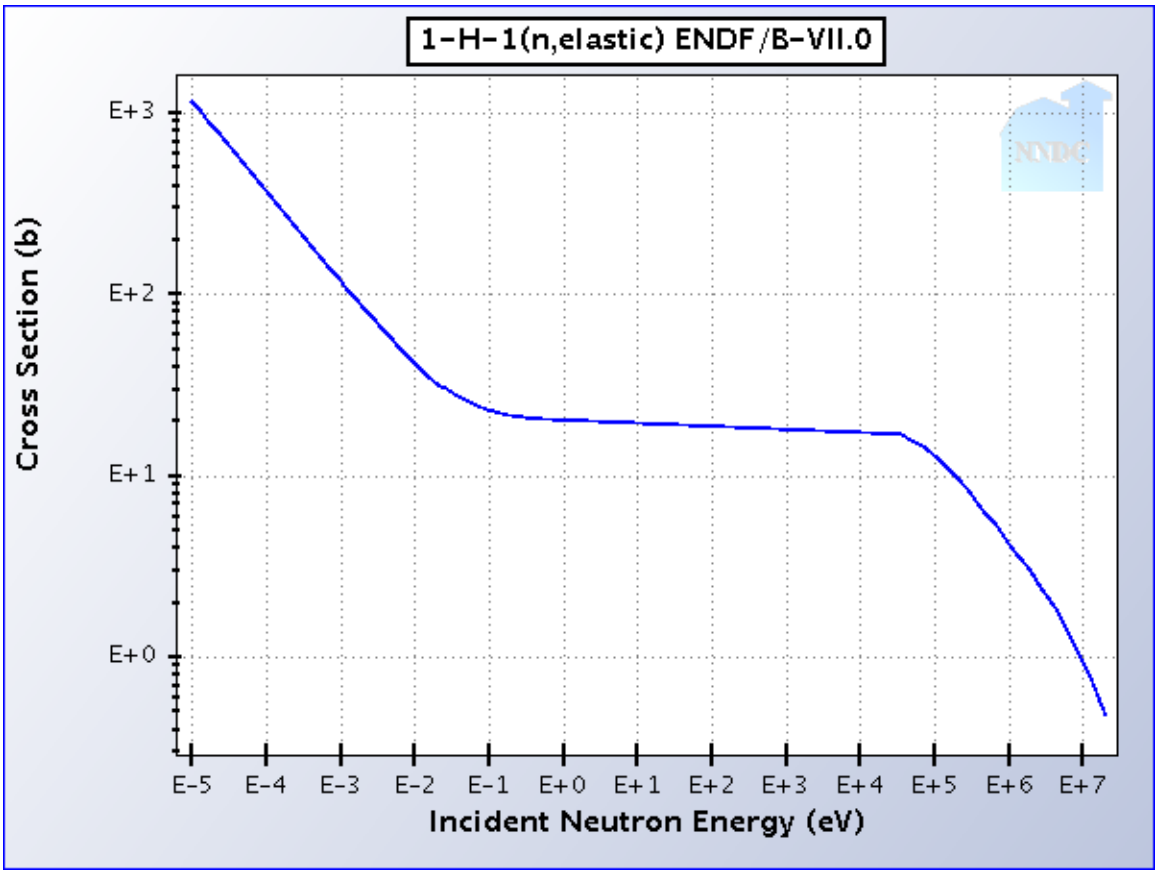

Figure E.1. Cross section vs. neutron energy for the ^{1}H(n,elastic) reaction.

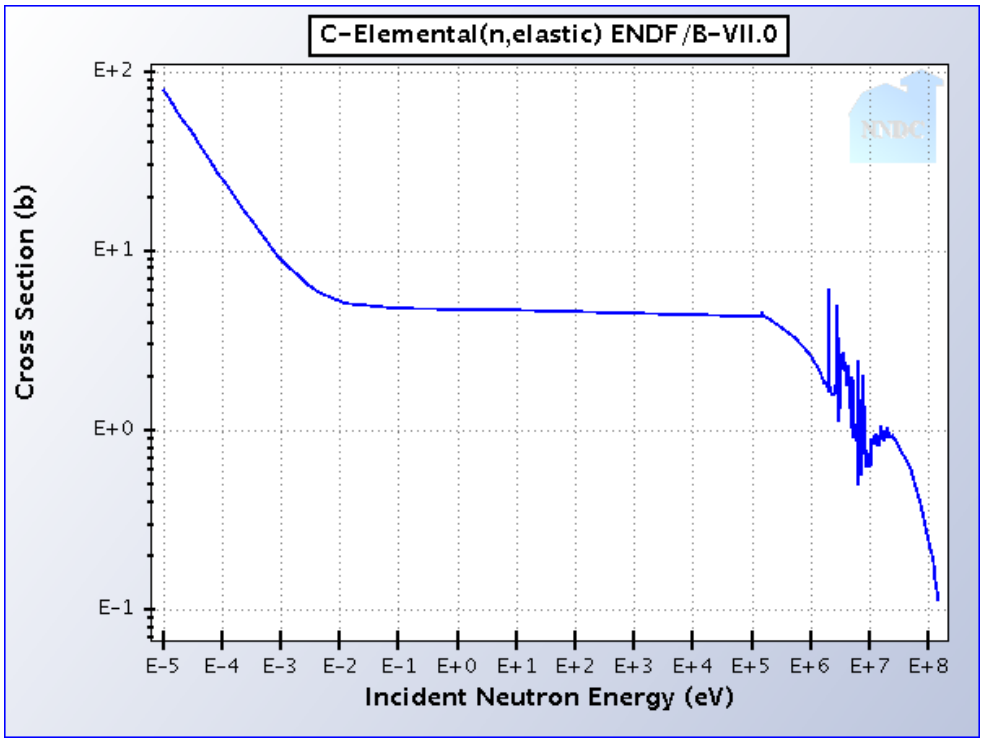

Figure E.2. Cross section vs. neutron energy for the ^{12}C(n,elastic) reaction.

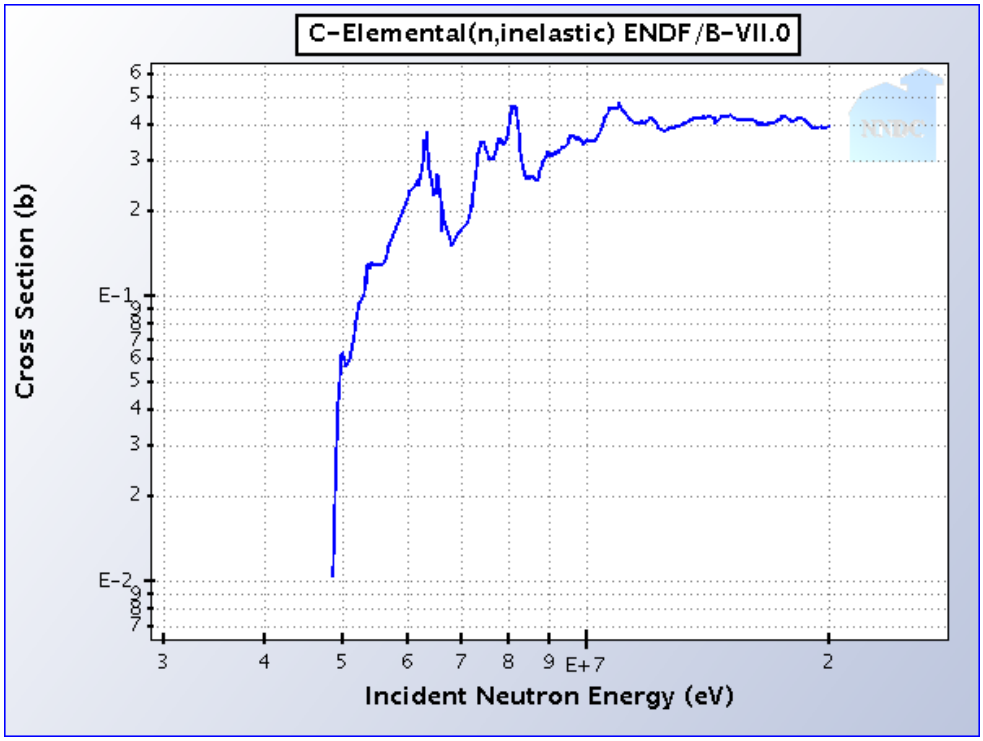

Figure E.3. Cross section vs. neutron energy for the ^{12}C(n,inelastic) reaction.

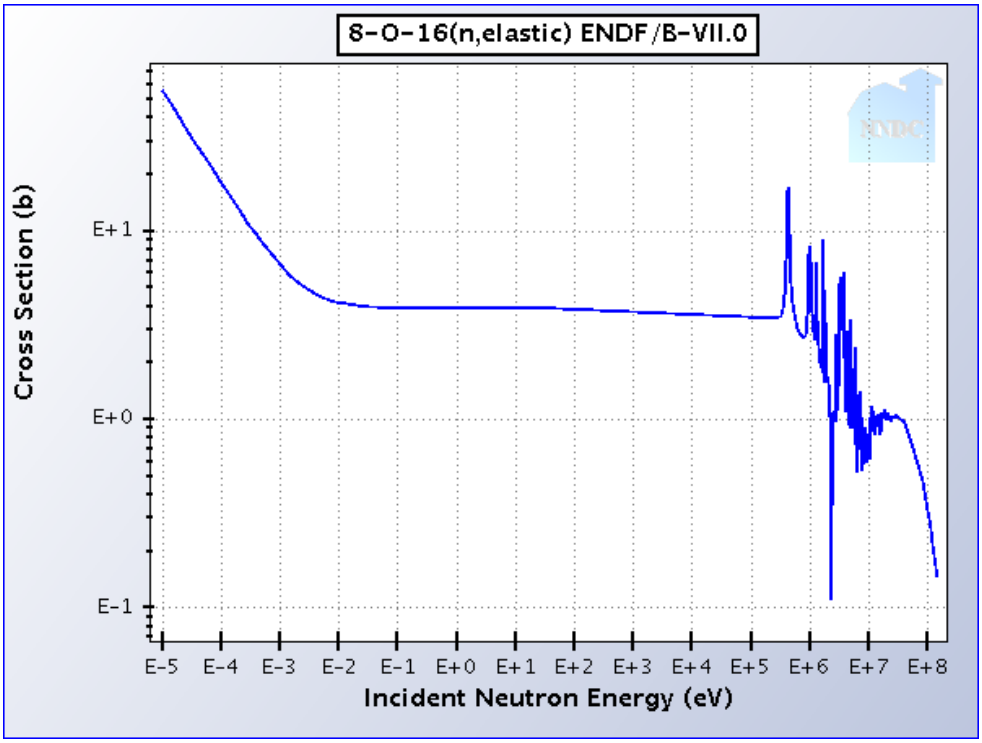

Figure E.4. Cross section vs. neutron energy for the ^{16}O(n,elastic) reaction.

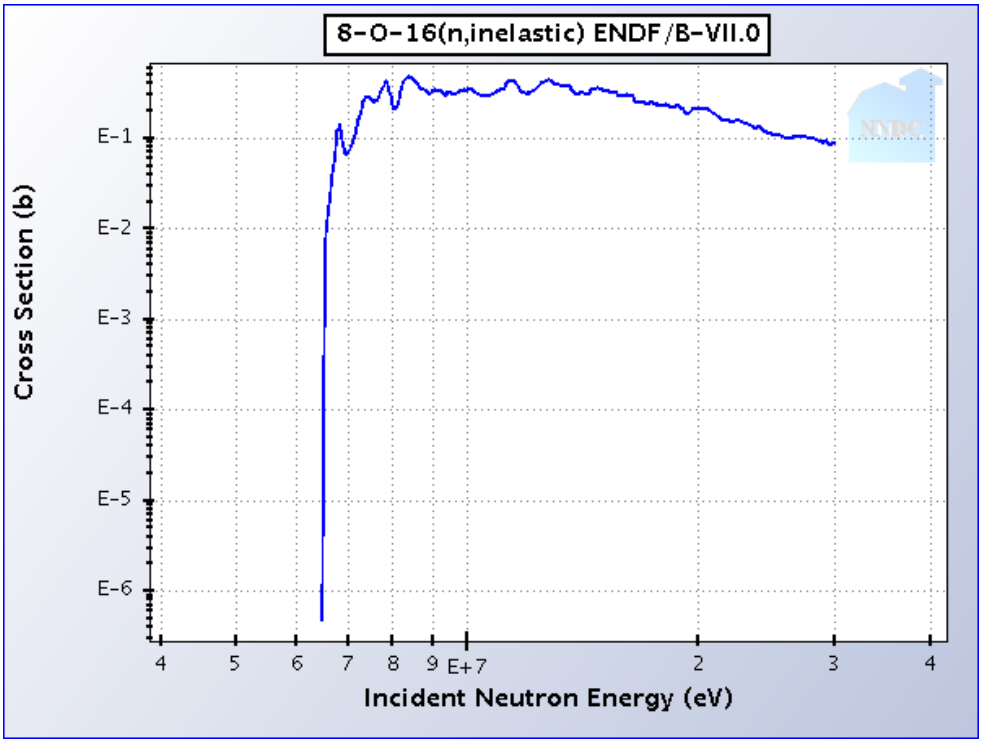

Figure E.5. Cross section vs. neutron energy for the ^{16}O(n,inelastic) reaction.

Appendix F - Gamma Dose Fraction Measurement Sources of Error

The following is a list of all uncertainties in the ionization chamber measurements for quantities whose uncertainty is 0.1% or greater.

Table F.1. Gamma Dose Fraction Measurement Sources of Error.

Quantity	Uncertainty
$Q_{T,TE}$ / $Q_{T,CO2}$	0.1%
N_c	2.0% (AAPM Recommandation)
$f_{t,c}$	0.5%
$A_{w,c}$	1.5% (Est.)
A_{TE} / A_{CO2}	2.6%
k_T / k_u (Exp.)	10%
Attenuation Correction	5.0% (Est.)
Distance Correction	5.0% (Est.)
Area Correction (Foil)	5.0% (Est.)
Gamma Dose Fraction (Ave.)	~ 100%
Dose Measured w/ TE-TE (k_T =1)	~ 5%*
Dose Measured w/ TE-TE (Exp. k_T)	~ 11%*

* The uncertainty in measurements with a single TE-TE chamber is dominated by the uncertainty in k_T. However, the uncertainty also varies to a lesser extent with the gamma dose fraction (DF). The uncertainties listed above assume a gamma dose fraction of 4%.

References

AAPM Report No. 7: Protocol for Neutron Beam Dosimetry. New York: American Institute of Physics, 1980.

Attix, F.H. *Introduction to Radiological Physics and Radiation Dosimetry*. New York: Wiley, 1986.

Baldock, C., Y. De Deene, S. Doran, G. Ibbott, A. Jirasek, M. Lepage, K. B. McAuley, M. Oldham, and L. J. Schreiner. "Polymer Gel Dosimetry." *Physics in Medicine and Biology* 55.5 (2010): R1-R63.

Baltas, Dimos, Nikolaos Zamboglou, and Loukas Sakelliou. *The Physics of Modern Brachytherapy for Oncology*. Boca Raton: Taylor & Francis, 2007.

Brady, Samuel Loren. *Development of Radiochromic Film for Spatially Quantitative Dosimetric Analysis of Indirect Ionizing Radiation Fields*. PhD. Dissertation, Duke University, 2010.

Drosg, M. DROSG-2000, Codes and database for 59 neutron source reactions, documented in the IAEA report IAEA-NDS-87 Rev. 9 (May 2005), received from the IAEA Nuclear Data Section.

Fitzler, Andreas. TV, Code for curve fitting and analysis of nuclear spectroscopy data. 12 Aug. 2003. Web. 2011. <http://www.ikp.uni-koeln.de/~fitz>

ICRU Report 26: Neutron Dosimetry for Biology and Medicine. Washington: International Commission on Radiation Units and Measurements, 1977.

ICRU Report 46: Photon, Electron, Proton, and Neutron Interaction Data for Body Tissues. Bethesda, Md., U.S.A.: International Commission on Radiation Units and Measurements, 1992.

Knoll, Glenn F. *Radiation Detection and Measurement, 3rd Edition*. New York: Wiley, 2000.

Manglos, S. RKIN, Code for calculating relativistic kinematics for two-body nuclear reactions., 1980. Modified by B.C. Karp (1982). Modified by R.M. Prior (2000).

National Nuclear Data Center (NNDC). Web. 2011. <http://www.nndc.bnl.gov>

National Institute of Standards and Technology (NIST). Web. 2011. <http://www.nist.gov/pml/data/xraycoef/index.cfm> <http://physics.nist.gov/cgi-bin/Star/compos.pl>

Roberts, Mark. MAGNET, Code for calculating 20-70 magnet settings for neutron production via. ^{2}H(d,n) at TUNL. Modified by H.R. Setze (1992). Modified by Paul Huffman (1994).

Swartz, Brian W. *Characterization of neutron beams produced using the ^{2}H(d,n) reaction for determining dose to small animals*. M.S. Thesis, Duke University, 2007.

Taylor, G. C., J. T. M. Jansen, J. Zoetelief, and H. Schuhmacher. "Neutron W Values in Methane-Based Tissue-Equivalent Gas Up to 60 MeV." *Radiation Protection Dosimetry*. Vol. 61, No. 1-3, pp. 285-290 (1995).

Uusi-Simola, Jouni, Sami Heikkinen, Petri Kotiluoto, Tom Serèn, Tiini Seppälä, Iiro Auterinen, and Sauli Savolainen. "MAGIC polymer gel for dosimetric verification in boron neutron capture therapy." *Journal of Applied Clinical Medical Physics* Vol. 8, No. 2 (2007).

Waterman, F. M., F. T. Kuchnir, L. S. Skaggs, R. T. Kouzes, and W. H. Moore. "Energy Dependence of the Neutron Sensitivity of C-CO_2, Mg-Ar and TE-TE Ionisation Chambers." *Physics in Medicine and Biology* Vol. 24, No. 4, pp. 721-733 (1979).